A study on the statistical convergence of turbulence simulations around a cylinder

Special Issue of the 8th International Conference on Lyophilization – Freeze Drying (ISL-FD 2017)

R. Pisano & T. De Beer, Eds

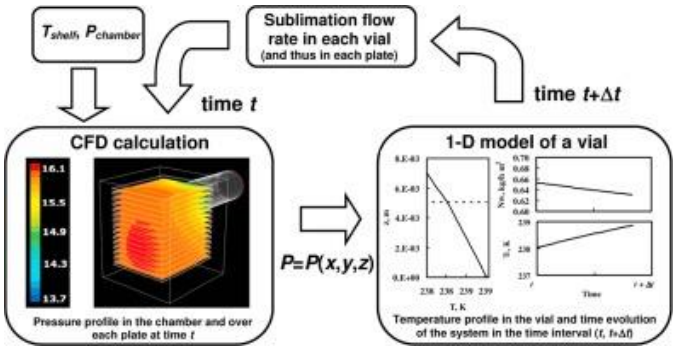

Use of Computational Fluid Dynamics for improving freeze-dryers design and process understanding. Part 1: Modelling the lyophilisation chamber

Antonello A. BARRESI[1*], Valeria RASETTO[1+], Daniele L. MARCHISIO[1]

[1] Politecnico di Torino

Institute of Chemical Engineering - Department of Applied Science and Technology

C.so Duca degli Abruzzi 24, I-10129 Torino, ITALY

*Corresponding author: Antonello Barresi (antonello.barresi@polito.it)

authors' e-mail: antonello.barresi@polito.it, valeria.rasetto@gmail.com, daniele.marchisio@polito.it

Abstract: This manuscript shows how computational models, mainly based on Computational Fluid Dynamics (CFD), can be used to simulate different parts of an industrial freeze-drying equipment and to properly design them; in particular, the freeze-dryer chamber and the duct connecting the chamber with the condenser, with the valves and vanes eventually present are analysed in this work. In Part 1, it will be shown how CFD can be employed to improve specific designs, to perform geometry optimization, to evaluate different design choices and how it is useful to evaluate the effect on product drying and batch variance. Such an approach allows an in-depth process understanding and assessment of the critical aspects of lyophilisation. This can be done by running either steady-state or transient simulations with imposed sublimation rates or with multi-scale approaches. This methodology will be demonstrated on freeze-drying equipment of different sizes, investigating the influence of the equipment geometry and shelf inter-distance. The effect of valve type (butterfly and mushroom) and shape on duct conductance and critical flow conditions will be instead investigated in Part 2.

Keywords: Computational Fluid Dynamics; Freeze-dryer; Lyophilisation; Equipment design; Multi-scale modelling.

List of abbreviations

BE	Boltzmann Equation
CFD	Computational Fluid Dynamics
DSMC	direct simulation Monte Carlo
DVM	Discrete Velocity Method
LBM	Lattice Boltzmann Method
TDLAS	Tunable Diode Laser Spectroscopy
QbD	Quality by Design

1. Introduction

Freeze-drying is a fundamental process in pharmaceuticals manufacturing, as it is carried out at low temperature and thus allows preserving most of the critical quality attributes of the product during the removal of the water (or of the solvent used); this is necessary to guarantee the required shelf stability to many drugs and pharmaceutical products. The target of the process is to get the desired value of residual moisture in the final product, with the required appearance and cake structure, maximizing the sublimation rate; in fact, lyophilisation is an expensive process and the drying time must be minimised to maximize plant productivity and reduce the cost of the product.

The design of the equipment can have a strong influence on the final product quality, as it will be shown in the following. In addition, the selection of the operating conditions required to obtain the desired product characteristics, may be significantly influenced by the equipment design (chamber, duct and valve, condenser) and affects the minimum drying time. In fact, robustness of the cycle and drying process time reduction are conflicting goals, as the drying rate increases if the operation is carried out at higher temperature and higher chamber pressure, increasing in turn the heat transfer rate from shelf to product in vials or trays (Pisano et al., 2011a). To operate at higher pressure and temperature increases the risk of trespassing the limit product temperature, and thus failure of the processed batch.

Finally the reliability of the operation depends not only on the cycle robustness (Fissore et al., 2012b; Pisano et al., 2013; Bosca et al., 2015) but on the quality of the monitoring and control system (Barresi et al., 2009; Fissore and Barresi, 2011a; Fissore et al., 2018; Bosca et. al., 2017) and on the proper design of the apparatus. It is important to have a deep knowledge and understanding of the process and of the influence of the different variables and operating conditions, to avoid choices and decisions that would compromise the final product quality: this is the application of the "Quality-by-Design" (QbD) concept, according to which quality should be built in the process, with a proper design of equipment, process control and set up and not only verified at the end (Barresi et al., 2008b) [an account for earlier references can be found in Barresi et al. (2010b) and Fissore et al. (2015)].

One factor that must be accounted for, is that local process variables, that significantly influence the drying of single vials, not only depend on the selected set points of the operating variables, but are strongly influenced by apparatus geometry and design, equipment size and loading: this explains why problems and failures, may be experienced with sensitive products when transferring the process from one equipment to another. Local pressure values are particularly important, because the system responds very quickly to an increase in pressure with an increase in the product temperature; as a matter of fact, the undesired pressure profile is the top event with the highest probability, if a risk analysis is carried out, and the one with the worst consequences (Bosca et al., 2017). Difficulties and failure can occur also when the loading in the same equipment is changed, because it can change the cake resistance, the contribution of radiating heating, or the hydrodynamics in the apparatus (Fissore et al., 2009; Fissore et al., 2012a).

Much more severe may be the problem in case of process scale-up from a laboratory or pilot equipment to the industrial one [see for example Jennings (2002), Barresi (2011), Fissore and Barresi (2011b) and previous references in the last paper]. It has been shown that modelling tools and an advanced control system may be extremely useful to manage the scale up process; but also

in this case the appropriate location of the sensors, and the correct interpretation of their reading is essential and to this purpose the knowledge of the fluid dynamics of the apparatus is of fundamental importance (Barresi and Pisano, 2013; Barresi et al., 2018).

When designing a freeze-dryer, two categories of critical issues must be properly addressed. The first category is related to the problem of batch heterogeneity; as it is well known, especially at the industrial scale, it is challenging to design an equipment capable of guaranteeing the very same operating conditions for the entire batch (Rasetto et al., 2008; Barresi et al., 2010a). Vials positioned in different points of the chamber experiences different temperature and pressure histories and this can lead to significant variations for the residual water content. The geometry of the chamber as well as temperature gradients of the heating fluid circulating through the shelves, are typical design and operating parameters affecting the batch heterogeneity.

Other issues are the capability of the freeze-dryer to evacuate the water vapour flow rate, in order to operate under the desired conditions (i.e., specific sublimation rates and thus batch drying times, and chamber pressure). This is related to establishment of sonic flow condition in the duct (Oetjen, 1999; Searles, 2004; Nail and Searles, 2008; Patel et al., 2010), which will be dealt with in Part 2 of this work (Marchisio et al., this issue), and to the proper design and operation of the condenser.

The investigation of these issues solely relying on experimental techniques is very costly and time consuming, therefore the use of computational models is an interesting alternative (Sharma et al., 2011) and a plethora of them are available. These are generally classified based on the Knudsen number, *Kn*, namely the ratio between the mean free path of the gas molecules (i.e. that between two subsequent molecular encounters or collisions) and the characteristics length of the equipment (Knudsen, 1909).

When the Knudsen number is much smaller than one, the fluid can be considered as a continuum and the standard continuity (mass conservation), momentum and energy balance equations can be solved by using tools developed in the Computational Fluid Dynamics (CFD) community. These are based on the solution of the governing equations with finite-volume schemes with no-slip boundary conditions at the walls (Batchelor, 1965).

This approach has been successfully employed to model the drying chamber, to investigate the internal fluid dynamics and gas composition, predict possible non-uniformity of the batch and critical aspects in scale-up and process monitoring (Barresi et al., 2008a; Rasetto et al., 2008; Rasetto, 2009; Rasetto et al., 2009; Barresi et al., 2010a; Barresi et al., 2010b); to predict the spatial variation of pressure over the shelf (Rasetto et al., 2010; Ganguly et al., 2017); to model flow in the cylindrical duct and to estimate conductance and calibrate the TDLAS measuring system (Alexeenko et al., 2009; Patel et al., 2010; Ganguly et al., 2012); to evaluate the effect of equipment modifications and valves and baffles positioning (Ganguly et al., 2013) and the fluid dynamics in different types of condensers (Petitti et al., 2013), in order to improve process and equipment performance.

In the so-called transitional regime (for Knudsen numbers bounded between 0.01 and 0.1) CFD equations are solved with slip boundary conditions at the walls (i.e. partial-slip boundary condition) due to the small number of collisions with the walls (Maxwell, 1879).

On the contrary, when the *Kn* number is larger than unity the continuum hypothesis is not valid anymore. Under these conditions the flow has to be described by Molecular Dynamics (MD)

simulations (Baback and Reese, 2014; Docherty et al., 2014) or by solving the Boltzmann Equation (BE). The BE is often solved with stochastic methods, as in the context of direct simulation Monte Carlo (DSMC) (Bird, 1994; White et al., 2017), or on a fixed lattice, as in the Lattice Boltzmann Method (LBM). These methods, although more expensive than standard CFD calculations, can be used to describe large-scale equipment, where the velocity distribution is out-of-equilibrium and not Maxwellian. DSMC, which is employable also in the transitional regime, has been used to model the chamber-to-condenser duct (Alexeenko et al., 2009) and the condenser, and was judged very efficient in describing also the icing phenomena that occur on the coils of the condenser (Ganguly et al., 2011; Ganguly et al., 2012; Ganguly and Alexeenko, 2012).

Another important technique used to solve the BE is based on the method of moments (Struchtrup, 2005), where the governing equation (i.e. the BE) is solved in terms of the moments of the velocity distribution, by resorting to ad-hoc closures (Grad, 1949) or on functional assumptions on the mathematical form of the distribution, as in quadrature-based moments methods (QBMM) (Marchisio and Fox, 2013; Icardi et al., 2012). It is useful to mention, however, that whereas DSMC and LBM can virtually reproduce any type of velocity distributions, the Grad method can deal only with small deviations from the Maxwellian distributions, resulting otherwise in non-physical velocity distributions. It is useful at last to mention the Discrete Velocity Method (DVM) (Nurlybaev, 1993) where the distribution is discretised in a number of velocity classes and the collision integral is replaced with a discrete version of it. DVM are however difficult to apply to complex geometries with realistic flow conditions.

Another very important point to be accounted for is the flow compressibility. Under moderate operating conditions the Mach number is smaller than unity and the flow is described with incompressible CFD solvers. Sonic flow conditions may typically occur in the duct, in correspondence of the reduced section of the valve, as mentioned before. In this case it is necessary to employ compressible CFD solvers, capable of dealing with sonic and super-sonic conditions and with shockwaves. Sonic flow may occur also in the chamber, in case of jet flow caused by leakage from small holes.

At last it is important to mention that simulations of typical freeze-drying processes should account for the interplay between the flux of sublimated solvent (in most cases water) coming from the product (either in vials or in an open tray), the evolution of the product itself and the local and instantaneous operating conditions in the chamber. Under some operating conditions it can be assumed that the sublimation rate is dictated by some manipulated variables. This is often called one-way coupling. However, very frequently the state of the product and the sublimation rate are controlled also by the flow conditions in the chamber (i.e. two-way coupling) as the product affects the solvent flow, but the flow in turn affects the product, and this situation can be described via a multi-scale modelling approach.

One strategy recently proposed is that of considering a pseudo steady-state, decoupling the dynamics of the product from that of the chamber. This is realized by running steady-state CFD simulations characterizing the flow field in the freeze-drying chamber at different phases of the freeze-drying cycle. Another possibility is to solve in advance the computational models related to the product under different operating conditions and pre-compile a look-up table. The effective coupling (in simulations) of the flow field and the product evolution is particularly important to estimate the evolution of product temperature and of residual ice content in the various vials

(Rasetto et al., 2010).

Other challenges are also offered in the simulation of freeze-drying operations. Two worth citing are: accounting for radiation and properly estimating thermodynamic and transport properties. The first one is usually tackled with simple (and empirical) approaches (see for example Pisano et al., 2008; Pisano et al., 2011b), whereas the latter is addressed by accounting for the translational, rotational and vibrational degrees of freedom of the solvent molecule (mostly water) and by resorting to the standard kinetic theory of gases (Sane et al.,2017).

The aim of this work is to review the potentiality of CFD showing how the results can be used in a QbD perspective, to get a deeper process understanding, to improve equipment performance at the design stage and to avoid errors in operation. It will be shown how the knowledge of the fluid dynamics in the chamber may be useful for the correct positioning of the monitoring sensors. Two-way coupling between fluid dynamics and process rate will be investigated by using a multi-scale model.

Literature results have evidenced that CFD can be a reliable tool for better design of freeze dryers, and its use has also been recently experimentally validated by Sane et al. (2017), comparing measured and predicted pressure profiles over a shelf. Anyway, very little is currently available in literature that can be used in particular for improvement of the batch uniformity and prediction of the duct conductance and choked flow conditions; the present work aims to fill at least in part this gap. In this paper the modelling of the freeze-dryer chamber will be dealt with, while duct and valve will be considered in Part 2. The condenser will not be considered in detail, as this type of equipment has been already investigated in a series of previous works. It must be evidenced that CFD can be useful also in this case for design purposes (and some examples will be shown in Barresi and Marchisio, 2018), but for the lower pressure conditions other approaches suitable for the transitional and free-molecular regimes may be preferable; in any case in this equipment the icing phenomena represent the most difficult task.

2. Governing equations

The fluid dynamics of the vapour in the drying chamber is described by the well-known continuity and momentum balance equations that, written in their general form (by using the Einstein notation) read as follows:

$$\frac{\partial \rho}{\partial t} + \frac{\partial}{\partial x_i}\left(\rho u_i\right) = 0 \tag{1}$$

$$\frac{\partial}{\partial t}\left(\rho u_i\right) + \frac{\partial}{\partial x_j}\left(\rho u_i u_j\right) = -\frac{\partial P}{\partial x_i} + \frac{\partial}{\partial x_j}\left(\tau_{ij}\right) + \rho g_i \tag{2}$$

where ρ is the fluid density, related to temperature and pressure values through the ideal gas law, that is a valid equation of state for the operating conditions investigated in this work, u_i is the i^{th} component of the fluid velocity, P is the fluid pressure, g_i represents field forces, such as gravity (negligible in this case), and τ_{ij} is the viscous stress tensor, that for Newtonian fluids is usually

expressed as a function of the fluid viscosity μ and of the velocity gradient tensor. As mentioned in the Introduction, viscosity and diffusion coefficients are usually calculated by resorting to the standard gas-kinetic theory and these equations are valid in the continuous regime when the *Knudsen number*:

$$Kn = \frac{\lambda}{r} \tag{3}$$

ratio of the molecular free path, λ, to a certain representative macroscopic length-scale of the flow, r, is smaller than one (Knudsen, 1909).

The Knudsen number depends on pressure; under very low pressures (i.e. smaller than 10 Pa for the case investigated) the flow may be in the transitional regime, depending on the shelf inter-distance, whereas under higher pressures the continuum regime may be assumed. An evaluation of the *Kn* number for the case studies investigated, as a function of the operating pressure, can be found in Barresi and Marchisio (2018).

2.1 Multi-scale modelling of freeze-drying processes

Multi-scale models can be divided in two categories: (1) off-line and (2) on-the-fly approaches. In the first case the primary drying model and the apparatus CFD model are solved separately, whereas in the second case they are solved simultaneously.

Various primary drying models can be used but, to reduce the overall computational cost, a spatially mono-dimensional model is used for the off-line approach, whereas a lumped zero-dimensional model is used for the on-the-fly approach.

Among off-line methods, one can choose between the Fully-Iterative Multi-scale Method (FIMM) and the Pre-Simulated Iterative Multi-scale Method (PSIMM), as briefly described before in Barresi et al. (2010b). In FIMM a sequence of CFD models and primary drying simulations are carried out separately. Each simulation (run with certain input variables) produces several outputs, that can be used as input for the next step. In particular, at a certain time instant, a specific sublimation rate is assumed and a CFD simulation is run. The CFD simulation provides the pressure values in the chamber, that are used as boundary conditions for the product model, providing updated sublimation rate values, that can be used to run a new CFD simulation. The FIMM is summarized in Figure 1. This approach has been used to evaluate the influence of the local operating conditions on single selected vials (i.e. typically where the pressure is the highest and the lowest) and on the variance of the whole batch.

PSIMM is instead based on the simple idea of carrying out in advance some fluid dynamic simulations of the chamber at different sublimation rates; the collected data is then used to derive a specific correlation between sublimation rates and pressure. Product model simulations are eventually carried out by using the correlation stored in the database. The detailed one-dimensional model of Velardi and Barresi (2008), taking into account also the heat transfer in the vial wall, has been used to model the dynamics of the product. An example of application of this approach has been previously presented by Rasetto et al. (2010).

On-the-fly approaches are instead based on the idea of solving a (necessarily) simple product model as the CFD simulation is running. This can be done by using simple (algebraic) models that relate the product temperature and the local fluid pressure with the sublimation rate (see for

example Hill and Sunderland (1971)). The algebraic model is often a non-linear equation that can be solved in the CFD code (via user-defined functions in the case of commercial codes) via for example the Newton's method. A zero-dimensional model derived from the so called URIF (Uniformly Retreating Ice Front) model (Toei et al., 1975; Kumagai et al., 1991), is used for the on-the-fly approach. The details of the model used are given in the Appendix.

3 Case studies and simulation details

Two different equipment sizes (a small-scale apparatus and an industrial-scale apparatus, see Figures 1 and 2) have been investigated to assess the influence of the design parameters on the fluid dynamics and on the pressure distribution in the drying chamber. For the small-scale apparatus three different positions for the duct have been considered: in the centre of the rear wall, on one side of the rear wall and on the bottom of the chamber (see Barresi and Marchisio (2018) for complete geometrical details). The laboratory-scale freeze dryer is constituted by four shelves (450 x 455 mm) for a total chamber volume of 0.2 m^3. The large-scale freeze-dryer contained 14-17 shelves of 1500×1800 mm for a total volume of 10.3 m^3 (with a 200 mm lateral channel) and a 800 mm diameter horizontal duct (duct length/duct diameter = 2).

Three different distances between the product and the upper shelf have been considered for the small-scale apparatus and four for the large-scale apparatus. In the small-scale chamber the number of usable shelves has been maintained constant, equal to 4, and the different distance between the shelves was determined varying the free space between the bottom of the chamber and the first shelf and that between the last shelf and the top of the chamber (see Figure 2). In the industrial chamber the number of usable shelves has been varied from 14 to 17, but the position of the first and of the last shelf was not varied. In Table 1 the values of the distance between the shelves, *h*, and of the clearance between the product and the upper shelf, *r*, considered for the simulations for both the small- and large-scale apparatus have been reported.

Table 1. Geometrical characteristics of the (L) industrial and (S) pilot scale drying chamber configurations.

Case	**Number of shelves**	**Shelf-shelf distance, *h* (mm)**	**Product-shelf distance, *r* (mm)**
L1	14 (+1)	110	67
L2	15 (+1)	100	57
L3	16 (+1)	93.5	50.5
L4	17 (+1)	85	42
S1	4 (+1)	100	57
S2	4 (+1)	60	17
S3	4 (+1)	50	7

The largest clearance corresponds to normal and usual conditions in practical cases, while narrower clearances may represent cases where larger loading are obtained increasing the number

of shelves or taller containers are used (in the simulations a constant thickness of the "product layer" has been considered). One of the goals of the work is also to assess the relevance of the boundary conditions, and in particular the effect of the slip, and its dependence on the clearance.

The three-dimensional simulations carried out in this work were based on structured computational grids of about 300,000 (for the small-scale apparatus) or 600,000 (for the large-scale apparatus) hexahedral cells, representing the geometry of the freeze-drying chamber by using standard numerical methods. The commercial CFD code Ansys Fluent was used.

Inlet boundary conditions were set for the sublimation surfaces, corresponding to the vials placed on each shelf, while a standard pressure-outlet boundary condition was used for the final section of the duct connecting the chamber to the condenser.

Most of the cases investigated included only water vapour as solvent, but in a few selected test cases injection of inert gases (i.e. nitrogen) at different flow rates, to control the chamber pressure, was also simulated.

The chamber walls were considered at 283 K, with a shelf temperature of 258 K.

Steady-state simulations of the primary-drying phase have been carried out considering the maximum available sublimation rate of 1 kg m^{-2} h^{-1} with an interface product temperature of 239 K; other simulations have been also carried out at different sublimation rates (from 0.50 kg m^{-2} h^{-1} to 0.90 kg m^{-2} h^{-1}). The temperature of the vapour was assumed equal to the temperature of the sublimating surface (T_i).

Some scalar transient simulations have been also carried out to investigate the dynamic response of the small apparatus to variations of the sublimation rate on the different shelves; the details will be given in section 4.2.

Further simulation details can be found in Barresi and Marchisio (2018).

For the dual scale model, the freeze-drying of a 5% solution of bovine serum albumin, buffered with tris-HCl 01 M, in vials having a total volume of 4 ml, internal diameter of 12.24·mm, mean glass thickness of 1 mm and maximum air gap at the bottom of 0.7 mm, has been considered as test case.

4. Results and discussion

4.1. Steady state chamber modelling

4.1.1. Effect of duct location and assessment of flow regime.

CFD can be used to test different design solutions, for example the position of the duct connecting the chamber to the condenser, whose effect depends also on the distance between shelves. The influence of the duct position has been studied in a systematic way in the small apparatus: here three different locations are considered, at three different shelf clearances in order to obtain a general conclusion to be used as a guideline.

In Figure 2 (upper graphs) an example of the contour plots of the velocity magnitude has been reported for two different positions of the duct; the complete velocity and pressure data set, for the three geometric configurations, is given in Figures 6 and 7 in Barresi and Marchisio (2018). For these contour plots it can be observed that the maximum of the velocity is reached near the duct; moreover, when the duct is positioned at the bottom of the chamber, stronger velocity gradients are

observed. In all the investigated cases, the vapour moves from the front of the chamber to the back and when the duct is positioned in the centre of the rear wall the flow field becomes symmetric with respect to the plane *x*-*z*. The vapour flow field becomes less dependent on the apparatus geometry also when the clearance between the shelf is reduced.

Figure 2 (bottom graphs) also shows the pressure distribution over the shelves for the same two geometries and different shelf clearances. As it is seen, when the clearance between the shelves is large, and the shelf has a small size, the pressure difference between the centre and the edges of the shelf is quite limited; in this case it is more influenced by the position of the duct as is the flow field. On the contrary, when the shelf-to-shelf distance is quite small, or the size of the shelf increases, as in the industrial apparatus, the pressure difference between different points of the chamber becomes significant, but it is weakly affected by the position of the duct (as proved by the fact that profiles are in this case only slightly asymmetric).

It has been shown that, at least in the first part of the transition regime, the one close to the continuum one and characterised by *Kn* of the order of 0.1, which is called the "slip regime", the gas velocity at the solid surface is different from that of the wall (which is zero). Thus it is possible to describe the fluid dynamics using the same equations for mass, momentum, and energy balance, but slip boundary conditions. If the Maxwell's model is used, the following equation is used for the tangential component slip (the normal component is still equal to the wall normal velocity) (Maxwell, 1879):

$$u_{j|wall} = \left(\frac{\alpha_v - 2}{\alpha_v} \right) Kn\, r \frac{\partial u}{\partial z} \qquad j = x, y \tag{4}$$

Of course in a discretised system the value of the gas velocity in the centre of the computational cell is calculated, and the gradient can be given referring to this value and to the distance of the centre cell from the wall; α_v is the momentum accommodation coefficient of the gas (a mass fraction weighted average is used in case of gas mixtures).

It must be remembered that in the slip regime not only a velocity, but also a temperature jump will occur at the wall:

$$T_{gas|wall} = \left(\frac{\alpha_v - 2}{\alpha_v} \right) Kn\, r \frac{\partial T}{\partial z} \tag{5}$$

The simulations, with and without the low pressure boundary slip option activated have been compared to evaluate the relevance of the required correction in very limit conditions (in industrial applications it is hard to realize clearances narrower than those considered here). It must be taken into account that pressure drops increase with shelf size, but the correction will be proportional. In any case the slip at the wall reduces the friction, and thus the values estimated with the continuum hypothesis (and no slip boundary conditions) for the pressure drop will be in excess (and thus on the safe side for design applications).

The results shown in Figure 3 refer, between the cases considered, to the narrowest shelf clearance (7 mm). This is a very small value, and this is the cause of pressure drops significantly higher than those generally observed.

The situation is similar in all the clearances. In Figure 3 (top graph) the profile across the whole chamber, including the free lateral zone between shelves and wall, is shown in one case. As

expected, the pressure is slightly higher when calculated with the no-slip condition, but the profiles are very similar, with maximum values reached in the same position in the two cases.

It is interesting to notice that in the pressure and temperature ranges considered for water vapour, in the clearances between the shelves the Knudsen number is always larger than 0.01: the transitional regime is present and thus it is reasonable to use the low pressure boundary slip option in the viscous model.

Similar behaviour, but with progressively reduced differences, are observed with larger clearances. In particular, for the larger clearance considered in this work, no significant differences can be noted adopting the slip or the no-slip conditions.

As concerns the velocity patterns, the highest values occur in the free spaces between shelves and chamber walls. No significant differences can be appreciated in the velocity patterns when the low pressure boundary slip condition is adopted in the laminar model.

An increase in the values of the u_x and u_y velocity components can be observed (Figure 3, middle graphs) as a consequence of the slip in the upper part of the clearance (please note that a different condition was adopted for the lower plane, that is a source of water vapour). It can be also noted that the slip velocity at the wall is very significant in these conditions. It must be remembered that the relative velocity of the gas at the wall, in the slip regime, corresponds to a temperature jumps, as shown in the bottom graph of Figure 3.

The estimation of the average chamber temperature is relevant for example for the application of the pressure rise methods used to monitor product temperature (Milton et al., 1997; Velardi et al., 2008; Fissore et al., 2011); as this value is not generally available, it is assumed to be equal to that of the product, or an average between the shelf and product temperature. The CFD simulations can be used to estimate the influence of the assumptions done on the estimated product temperature.

An example is shown in Barresi and Marchisio (2018) (see Figure 8). It can be seen that the temperature of the wall (and the boundary conditions) directly affects the gas temperature in the clearance between shelves and wall, but not the temperature profile in the zone above the shelf. This latter one is determined by the sublimation process.

4.1.2. Fluid dynamics in the large-scale apparatus and effect on batch variance

Data on the flow field in the apparatus and on the distribution of the vapour flow over the shelves can be found in Barresi and Marchisio (2018) [see Figures 9-10]. The flow field and the pressure distribution in the lateral clearance and in the duct will be analysed in more detail in the Part 2 article.

The value of the pressure in the drying chamber is one of the most important parameters for the lyophilisation process and its effects on the mass and heat transfer involved in the process are quite complex. Decreasing the pressure chamber, the sublimation rate should be favoured (because increases the water partial pressure difference between the product interface and the chamber, and thus the driving force) but the efficiency of the heat transfer by conduction in the gas meatus between the vial bottom and the heating shelf decreases. The objectives for an optimal process design is to carry out the primary drying step with operating parameters (pressure and shelf temperature) that minimise the primary drying time maintaining the quality target of the product.

In the large-scale apparatus the number of shelves placed inside the drying chamber is much larger than in the small-scale chamber and two zones can be distinguished with this duct

configuration, respectively far and close to the duct. The pressure profile over the shelves at the bottom of the chamber, far from the duct inlet, is the most uniform one observed; moving up, the pressure distribution over the plate becomes less uniform. In particular on the plate near to the duct inlet the pressure reaches the minimum value observed in the system.

In the inset of Figure 1 a 3D draw of the chamber for the configuration L1 (h = 110 mm) is shown; in particular the pressure contour plot for all the plates has been computed. From this global view of the chamber the two different zones of the chamber (far and close to the duct) can be easily identified: in the first zone the plates from the 1st to the 9th are involved and the maximum pressure value is reached (red zone in the colour map); the zone close to the duct involves from the 10th to the last plate, and here the minimum pressure value (13.7 Pa) is reached (blue zone in the colour map).

An example of the pressure profile over the shelf in the two zones is given in Figure 4 (upper and middle graph), showing also the influence of the sublimation rate.

All the simulations have been carried out imposing the outlet pressure at the end of the duct, and thus are representative of the conditions that would establish in the chamber without a control action.

The pressure variation, at a given sublimation flow rate, is also strongly influenced by the average pressure in the chamber, as shown in Figure 4 (bottom graph) for two different shelves, because this affects gas density, viscosity and velocity. Actually the pressure drop is inversely proportional to the absolute pressure (Rasetto et al., 2010). Thus it is very easy, once the pressure profile is known, to calculate the one expected, in the same geometry, and at the same sublimation flux, at a different chamber pressure.

Results also highlight the presence of pressure gradients in the chamber. This aspect is important because the reading of the pressure sensors must be considered only as a reference pressure and pressure over the shelves may be higher; the relationship is not simple anyway and depends on chamber geometry and sensor location.

If the duct connecting to the condenser is located on the bottom of the chamber, a configuration generally adopted when a TDLAS sensor is installed, smaller variations along the shelf are expected, similarly to what shown for the smaller chamber (see Figure 2). On the other hand, the large and growing flow that passes in the lateral clearance will cause stronger vertical gradients in the average pressure over the shelves.

The whole set of pressure contour plots obtained for the different configurations has been analysed, in order to obtain the position of the maximum in the pressure profile (that depends on the shelf considered and on the relative position of the duct) and the maximum pressure drop observed (at the flow rate considered).

In Figure 5 (a) y_{max}, the y-coordinate of the maximum pressure value for each shelf is reported for all the configurations as a function of the vertical position of the shelf (z), whereas the maximum pressure difference over the shelf is shown in Figure 5 (b).

It is useful to remind that the four investigated configurations correspond to 14 (L1), 15 (L2), 16 (L3) and 17 (L4) usable shelves. As it was seen, for the shelves closer to the condenser duct, the position of the maximum pressure value is shifted to the rear corner of the shelf; however, when the number of the shelves increases, this shift is less marked.

Although the number of shelves below the duct is higher than the number above it, it is clear that the profiles are symmetric with respect to the horizontal plane passing for the duct. This is evident also in Figure 5 (b); the maximum pressure drop is observed near the condenser duct and decreases moving away from it.

It is also interesting to highlight that, as evidenced in Figures 5 (a) and (b), the shape of the curves is the same for all the configurations, independently of the number of shelves and the curves are parallel. In particular, increasing the number of shelves the pressure gradients over the shelves increase (because the clearance decreases) and the location of the pressure maximum get closer to the geometrical centre of the shelf.

Very important is also the effect of the sublimation rate, as already shown in Figure 4. The effect of the mass flow rate on y_{max} and ΔP_{max} is shown in detail in Marchisio and Barresi (2018) [see Figure 11]. The major effect of the mass flow rate is to increase ΔP_{max}, but this increase is larger for the shelves close to the duct.

It has been shown that the pressure variation is a function of the sublimation flow rate, and is influenced by the average pressure in the chamber, but in order to get a more general information, it is possible to consider the local pressure increase, that is the difference between the total local pressure and the value at the shelf border (ΔP). Thus it is possible to obtain, for selected positions on the shelf of interest (and of course for a specific geometrical configuration and for a selected shelf) correlations for pressure drop at a reference pressure. This method is the one successfully adopted in the FIMM multi-scale approach in the work by Rasetto et al. (2010).

From a theoric approach it is possible to explicitate the relationship between ΔP, the pressure variation along the shelf, and the relevant variables: the sublimation flux on the shelf, J_w, the distance along the shelf, L, the reference pressure in the chamber, P_{ref}, and the actual clearance between the shelves, r:

$$\Delta P \propto \frac{J_w L^2}{P_{ref} r^3}. \qquad (6)$$

As pressure reference, the pressure in the zone far from the duct is considered, and should correspond to the pressure "measured" in the chamber. The “distance along the shelf”, L, is the distance from the location of the maximum to the shelf border; it can be half of the shelf size if the duct is not influencing the profile, and becomes closer to the shelf size for the part of the shelf close to the duct. For shelves sufficiently large to reduce the relevance of the border effect, and not strongly influenced by the duct, the CFD simulations have confirmed the validity of the correlation given below; these are all the shelves in case of duct on the bottom of the chamber, like in the case investigated by Ganguly et al. (2017), or the shelves closer to the bottom for configurations similar to that investigated in this work.

If the pressure profile is not disturbed by the duct location, it is symmetric; in this case the maximum overpressure over the shelf and the maximum pressure difference along the shelf coincide, and can be easily calculated by correlation (6). If this is not true, the pressure distribution changes over the different shelves, as shown in Figure 5; the correlation still holds, but the location of the maximum is not known, and CFD simulations must be carried out on the geometry considered.

These results are in agreement with previous theoric and computational findings by Zang and Liu (2012) and Ganguly et al. (2017). Pressure differences smaller than 1 Pa were experimentally measured in small scale equipment by Sane et al. (2017); similar values were measured also by our research group (unpublished data). On the other hand, simulations and calculations evidence that in a large apparatus, with high sublimation rates and very narrow clearances, differences of several Pa can occur between different points of the shelves.

The approach described will allow for example to quantify the degree of uniformity that can be obtained in different conditions, and to compare in this respect different pieces of equipment. Calculating the variance of the curves (an example will be shown in the next section) it is also possible to lump in a single number to use as an index these characteristics, even if this has to be done with great care, because the complexity of the system can hardly be condensed in a single parameter.

It must be said that generally the effect of pressure gradients along the shelf on product temperature and drying rate is small, and overall much smaller than that caused by temperature gradients on the shelf; radiation from walls or windows (and especially with Plexiglas port) may be responsible for stronger non-uniformity (Pisano et al., 2008). It is surely negligible in lab scale apparatus, for the small size of the shelf, the small vapour flow even at high sublimation rate, and generally the large clearance. Sane et al. (2017) evidenced that the pressure gradient may also be beneficial, increasing the uniformity of the batch on scale up: in fact, higher pressure in the centre of the shelf causes higher temperature, and this can counterbalance the effect of wall radiation on edge vials. But they also highlighted that the final results depends on drying conditions and product resistance, and scale up effect might compromise the product quality in some cases.

In any case the results of this work have evidenced that the configuration with side duct can lead to larger intra-shelf gradients, but reduces inter-shelf pressure variations (compare Figure 2).

As concerns the evaluation of the shelf-to-wall distance effect, it must be taken into account that when the clearance between the shelves and the wall of the chamber decreases, the contribution of the radiation heat should not change. In fact, from the point of view of the vials, the walls of the chamber are always infinite walls and thus the view factor does not change.

The effect on the gas flow of the radiation from the wall has also been considered, comparing the results obtained with two different simulations (considering or not the contribution of the radiation with the P1 model) for the large-scale apparatus with 14 usable shelves (data not shown). The flow field of the vapour inside the chamber in the two cases is practically the same and so we can conclude that the effect of the radiation on the vapour can be neglected.

Much more important is the effect of the clearance between the walls and the plates on the fluid dynamics of the vapour. Figure 6 (upper graph) shows the evolution of pressure along a line crossing the shelf, the clearance wall and running along the centreline of the duct. It is confirmed that for the conditions and the geometry considered, also for the industrial scale apparatus, the pressure drop in the chamber may be negligible, and the largest part of the pressure drop occurs in the entrance zone of the duct, where the flow is strongly accelerated.

Considering the shelf aligned with the duct axis, the maximum in the pressure profile is hardly detectable, as the effect of pressure decrease due to the duct is much more relevant: as a result the maximum pressure difference over the shelf, in the range tested, can be higher than 2 Pa, and values of this order can affect batch uniformity, as already discussed. The maximum pressure variation in

the chamber is even higher, because a further decrease in the zone between shelves-pack and wall occurs.

The lower graph in Figure 6 evidences the contribution of the chamber to the total flow resistance; for comparison purposes the contribution of the duct is also shown. Anyway it is possible that for very narrow lateral clearances, they become the bottleneck of the system. A detailed simulation should be carried out for the geometries considered, evaluating also the influence of the product loads in the freeze-dryer and varying the distance between shelves.

4.1.3. Distribution of inert gases and solvent vapours in the drying chamber

Another important factor to consider when designing freeze-drying equipment is the presence of composition gradients in the vapour inside the chamber, due to spatially heterogeneous partial pressure of solvent (water or organic), as already discussed by Mayeresse et al. (2007). The introduction of an inert gas in the drying chamber is typically used to control and maintain the pressure at the value set for the cycle. As preliminary results (Barresi et al., 2008a, 2011a) suggest that the chamber cannot be considered as an homogeneous system, several simulations have been carried out in order to evaluate the inert gas distribution.

The results presented in Figure 7 have been obtained for a pilot scale drying chamber where the inert gas inlet has been supposed positioned in the top corner of one of the lateral walls of the chamber. The system seems to be segregated; that is, the composition of the atmosphere in the chamber in not everywhere the same. High inert gas concentration values (red zones in the figures) are reached close to the inert gas injection, but the zone is always quite limited and confined.

For the pilot-scale apparatus, typical inert gas mass flow values during primary drying experimentally measured are about 17 sccm correspondent to $3.2 \cdot 10^{-7}$ kg s^{-1}, but values in the range $2 \cdot 10^{-8}$ to 10^{-6} have been frequently observed; in the secondary drying much higher values can be measured, as the desorption flux of the solvent has significantly lower values. For that reason simulations have been carried out in the range $1.20 \cdot 10^{-8}$–$1.20 \cdot 10^{-5}$ kg s^{-1} (see Figure 7); conditions for which a jet reaches the opposite wall have been also investigated [see Barresi and Marchisio (2018), Figure 13]. Cases shown in the first two images are more typical of actual conditions in primary drying (the case with lower flow rate is not shown, but is similar with even more localised gradients). The two bottom graphs of Figure 7 show the case of higher flow rate, when a jet forms crossing almost all the chamber (the maximum velocity in this case reach 380 m s^{-1}. Even in this case the higher concentration of inert gas is localised in the region in the proximity of the jet. Moreover, increasing the inert gas flow rate the segregation of the system does not decrease significantly. It is important to observe that at typically operating values the effect of the inert gas is very local; the atmosphere changes composition close to the injection zone (the maximum inert gas fraction varies from 0.7 to 0.8 and then to 0.59 in the cases shown), but all the inert gas is concentrated in the clearance between the gas inlet and the outlet of the chamber (duct). Even with much higher inert gas flow rates, the value of inert gas concentration in the space between the shelves remains limited (see Figure 13 in Barresi and Marchisio (2018)). In Figure 7 (bottom right) the region where the inert gas mass fraction is higher than the volume-averaged value is evidenced, for the third case shown; four surfaces corresponding to a fixed inert gas concentration (the first and the last differ by 100 times) are evidenced, highlighting once again the very strong and localised gradients.

The pressure remains quite uniform, even if it increases with the inert gas flow rate; further data for the high inert gas flow rate regime can be found Barresi and Marchisio (2018).

As the introduction of nitrogen in the drying chamber can affect both the heat transfer from the heating surface to the product, and the mass transfer from the interface of sublimation to the chamber (Mayeresse et al., 2007), product dynamics, i.e. the evolution of temperature and residual ice content, may be affected by the way used to control the pressure.

The prevailing effect when introducing nitrogen in the drying chamber is the decrease of the heat transfer coefficient, that reduces the amount of heat that is transferred from the heating surface to the product, and, thus, the sublimation flow. Product temperature is decreased, due to the lower partial pressure of water in the drying chamber. The consequence of the decrease of product temperature and of the heat flux is the increase of the time required to complete the primary drying.

Of course an opposite result would be obtained using an inert gas with a thermal conductivity higher than that of the water vapour; it can be mentioned that in the past the use of such gases has been proposed to speed up the process (Mellor, 1978; Elia and Barresi, 1998), but this practice does not seem to have got widespread use.

Obviously the real impact of the inert gas fraction depends on the actual distribution over the shelves, as discussed before, and CFD is essential for this evaluation.

Vapour and inert gas distribution, and vapour pathways, can strongly influence efficiency and performance of the condenser too; the inert gas mass fraction increases in the condenser approaching the outlet. Of course, optimal design of the condenser should guarantee the best performances in terms of both heat and mass transfer. This has been discussed in previous works (Petitti et al., 2013; Ganguly et al., 2013), but is out of the scope of this paper.

4.2. Transient chamber modelling and sensor response

The control of the process is very important, but in order to be effective the response of the sensors must be reliable. It has been shown that it may be important to take into account the dynamic response of the sensor, in case of pressure rise test (Pisano et al. 2017). But in order to implement the PAT suggested by the QbD (Quality by Design) philosophy, it is important to take into account the fact that the drying chamber has non-uniform conditions, and the influence that this and the internal fluid dynamics have on the measures of the sensors and on the response of model-based monitoring tools (Genin et al., 1996; Mayeresse et al., 2007; Rasetto et al., 2008).

In the previous section it has been shown that a strong variation of the inert gas fraction may be localised, but often the location of the Pirani sensor is close to the inlet of bleeding gas. The inert gas distribution can affect the Pirani reading and the estimation of the end point of the primary drying. Whereas Pirani is generally used only in low cost equipments (e.g. pilot scale apparatus), is quite widespread in conjunction with Baratron and their readings are used for estimating the end of the primary drying. Similarly, the line 2-3 in the inset of Figure 8b is the possible trajectory of a laser beam used for gas composition monitoring, but again in this plane the strongest gradients of inert gas concentration may occur, as previously shown in Figure 7.

The relevance of the location of other types of sensors, like the moisture sensor (Genin et al., 1996) or the cold plasma ionisation detector (Mayeresse et al., 2007), and its effect on the sensor reading, have been also evidenced in previous works or are currently under investigation, as for the

quadrupole mass spectrometer, whose application in freeze drying is expanding (Ganguly and Rhoden, 2017).

Thus it is important to characterize the drying chamber in order to evaluate the observability of the quantity of interest for both pressure and moisture sensors. To this purpose the determination of a process transfer function for the drying chamber could be interesting for all the devices (like those mentioned above) which provide a local measure of the property of interest.

The dynamic response of the open system when perturbing the system with a material disturb has been studied by mean of scalar transient simulations. These simulations are carried out for the fully loaded pilot scale apparatus (configuration S1) starting from the converged steady-state simulations previously presented and adding an inert scalar at the sublimation interface (sources ss_i). Four possible detection points in the chamber have been investigated (see Figure 8b). The effect of the diffusivity has been evaluated because it is important for the interpretation of measurements of solvent concentration in the chamber; in this case the scalar diffusivity has been assumed equal to the kinematic viscosity, as the Schmidt number can be considered equal to one. Details of the simulation plan are given in Table 3 in Barresi and Marchisio (2018).

The case with only one shelf loaded with product has been also investigated considering that, especially in pilot scale apparatus, reduced batches are used to develop optimal freeze-drying cycles. Moreover also the sublimation flux is varied because, as it has been highlighted in the previous sections, it can affect the fluid dynamics of the vapour in the chamber. Several different sources of disturb have been considered: on all the sublimation surfaces or on a specific shelf.

In Figure 8 (upper left) the simulations for an equal disturbance on all the shelves (considering or not the mass diffusivity, case D1 and D2) are compared. It can be observed that at high sublimation rates the diffusivity has no effect on the dynamic response of the system: in fact, the two curves are overlapped. In this case all the sensor points are suitable to detect the response, with very short delay. On the contrary, if the step disturbance is only on the third sublimating surface (D4), not all the points detect the disturbance, but only the one close to the duct. In this case the absolute value of the step disturb does not reach the unit value because it is diluted by the other vapour sources (Figure 8, upper right). This aspect is important in order to assess the proper position of the process monitoring sensors. To this purpose, another important aspect is the different dynamic response obtained at the different detection points. In fact, different response delays characterize the dynamic curves of the points; the differences are small at high sublimation rate, but very large differences are observed for different loads (compare simulation D4 and D11, in the upper right graph, with sublimation rate respectively 1 and 0.1 kg h^{-1} m^{-2}, and disturbance only on ss_3). It must be remembered that a typical pressure rise test lasts 5-20 seconds.

In Figure 8 (bottom left) the effect of the position of the source of the disturbance is shown. In these three cases the flow field in the chamber is that corresponding to full load at high sublimation rate but the disturbance was applied only to one of the shelves. As it can be expected, depending on the shelf selected for perturbation, the delay of the response detected in point 1 is different. The second information that can be taken from this graph is that the system can not be considered perfectly mixed; in fact the asymptote value of the response is different for the three cases and different from the expected value 0.25. Similar results were obtained for partially loaded systems.

Figure 8 (bottom right) shows the effect of the sublimation flow rate on the dynamic response of the system (for the full load system, simulations D1, D8 and D9). Decreasing the sublimation rate

both the response delay and the rise time increase.

Further results are shown in Barresi and Marchisio (2018) [Figures 16-19].

4.3. Multiscale simulations

Let us now discuss the results of the off-line multi-scale model reported in Figure 9. As previously mentioned, the off-line multi-scale model couples a CFD-based description of the entire freeze-drying chamber with a mono-dimensional model for the drying product (vial model). Only primary drying is considered here. The vial model tracks the evolution of the well-defined ice surface, which separates the dried product (or cake) from the product with ice crystals, still to be sublimated. The model also tracks the evolution of numerous properties (including the interface temperature) and is capable to predict, among other features, the remaining moisture content.

As mentioned, the off-line model takes the pressure values obtained from the CFD simulation and uses them as boundary conditions in the vial model, that is then run for each of the identified conditions. The multi-scale model is therefore capable of evaluating what each individual vial in the freeze-drying chamber does. These results are summarized in Fig. 9 in terms of the time evolution of the mean interface temperature among all the vials (top plots) and the standard deviation σ of the interface temperature (bottom plots) for two shelves, the bottom one (left side plots) and the twelfth one, close to the duct (right side plots).

For completeness, in the top plots the continuous line, representing the mean temperature, is plotted together with the dashed lines, representing instead the interface temperature evolutions for the coldest and hottest vials on the shelf. As expected, the interface temperature increases as the product in the vials dries, but due to the different flow fields of the evaporated solvent (water in this case) on the two shelves, the variance of the twelfth shelf is much larger than on the first shelf. This is due to the fact that the duct transporting the water vapour into the condenser is positioned right next to the 12th shelf, generating strong pressure gradients along the shelf. This is not true for the first shelf, that being far away from the duct, evacuates the water vapour more uniformly.

This difference is more evident in Figure 10 reporting results obtained with the on-the-fly multi-scale model. As previously mentioned, in this case a simple zero-dimensional vial model is implemented in the CFD simulation, evaluating (with a certain approximation) the local instantaneous sublimation flux based on the local instantaneous vapour pressure and temperature values, closing the two-way coupling between vials and freeze-drying chamber.

Figure 10 shows the contour plot on the top of the shelves (top plots) from two different view points (front versus back) in Pa and the sublimation fluxes (middle plots) in kg h^{-1} m^{-2}. It can be seen that the presence of the duct transporting the water vapour to the condenser creates a large gradient in the shelf pressure, resulting in a large gradient in the sublimation flux. As a consequence the vials close to the duct will dry faster, resulting in a heterogeneous distribution of the product properties in the different vials (among others the residual moisture content).

In the bottom plots of Figure 10 the sublimation rates over the twelfth shelf are shown in two cases, to compare quantitatively the effect of the pressure gradients over the shelf and of the fluid temperature variation inside the shelf. In the left plot a constant shelf temperature is considered, while in the right plot the temperature decreases by 2°C along the shelf. This evidences the relevance of temperature differences in the fluid along the shelf, highlighting the importance of a

good design that takes into account the maximum load in the apparatus (qualification tests are generally carried out at no load). The results also suggest that eventually pressure gradients might be counterbalanced designing a heat fluid path that creates a desired shelf-temperature gradient.

5. Conclusions

The effect of the geometrical parameters of the freeze-dryer chamber, i.e. the clearance between the loading shelves, the position of the duct, the clearance between the shelves and the walls of the chamber, the volume of the chamber, on the fluid-dynamics of the sublimated vapour in the drying chamber has been investigated. Interesting results have been obtained by mean of the computational fluid-dynamics for both the small scale and the industrial scale apparatus.

Typically, studying the freeze-drying process, uniformity problems for the batch are mainly related to the radiation effect, but also the fluid dynamics of the vapour in the chamber can affect the uniformity. The position of the duct that connects the drying chamber to the condenser determines the global flow field inside the chamber. The absolute pressure value, estimated over the vials, is affected by both the clearance between the shelves and the position of the duct. In particular the pressure increases if the clearance between shelves is reduced and the highest pressure value is reached by the vials far from the duct. This is important because different pressure values imply different product temperature and then different primary drying time so that some vials finish the sublimation phase earlier than others; in some cases this effect may be relevant.

Although the highest pressure values are reached when the duct is positioned at the bottom of the chamber, this one seems to be the best configuration from the point of view of the uniformity of the pressure over the plates. In fact, if the duct is positioned on the rear wall the non-evenness of the pressure over the plates close to the duct is higher than on the plates far from it.

It has been also observed, in the small scale apparatus, that the pressure profile over the plates does not change with the position of the duct if the clearance between the shelves is considerably reduced below the values that typically are used in industrial processes, but the absolute pressure increases. It can be also evidenced that in case of very small clearance, the flow can be in transitional regime, and when this happens a slip occur for the velocity at the wall, that reduces the pressure drop observed along the shelves.

Under similar operating conditions, the pressure values and the pressure differences (in different points of the same shelf or in different shelves) may significantly differ in two apparatuses of different size; higher values have been obtained by the simulations of the industrial scale apparatus, for the larger size of the shelves. Again, this will have as a consequence a different interface equilibrium temperature of the drying product and thus a different sublimation rate and final drying history of each vial.

These effects can be estimated by resorting to a two-scale approach, where the evolution of the product in each vial is linked to the mathematical description of the entire chamber. It has been shown how the influence of the local operating conditions on single selected vials and on the variance of the whole batch can be evaluated.

A model for the vapour source (the ice sublimation) can be directly implemented in the CFD code, if the focus is on the equipment design; an off-line approach, more suitable for process

transfer and scale up, based on the development of specific correlations from the results of preliminary CFD simulations, and on their coupling with a detailed model of the vial, has been also discussed.

The results obtained can be generalised, either to obtain a "fingerprint" of the piece of equipment considered, that can be compared to different ones, or to obtain correlations for the quantities of interest, that can be used for equipment or process design.

In a freeze-drying process of products in vial not only the flow field inside the chamber affects the operating conditions but also the stopper partially inserted in the vial may induce an important pressure drop depending on the sublimating rate and the shape of the stopper vent. Also differences in the positioning of the stopper may be relevant, as may be important differences in the shape of the vial bottom, which affects the heat transfer coefficient. This should be taken into account in the evaluation of the batch variance, as the contribution of the above mentioned factors may be comparable to that of the fluid dynamics investigated in this work.

Both the results obtained from the chamber and the vial simulations underline that the operating pressure specified by the cycle parameters and set during the primary-drying cannot be considered the true pressure of the system. In fact, the pressure is typically detected by means of sensors placed at the top of the chamber walls where the pressure can be higher or lower than the interface product pressure, depending on the vials position.

Concluding, these results can be useful not only for the apparatus design optimisation or for process transfer, but also to develop advanced model-based monitoring and controlling tools that typically do not take into account the property heterogeneity of the batch.

Acknowledgements

Part of this work has been financially supported by Telstar Technology S.L. (Terrassa, Spain) and Italian Minister of Education through a PhD fellowship (V.R.). Valuable suggestions and contributions from Miquel Galan (Telstar Technology S.L.), Miriam Petitti, Davide Fissore and Roberto Pisano (Politecnico di Torino) are gratefully acknowledged.

Supplementary material

Supplementary material and supporting data have been published in a *Data in Brief* paper (Barresi and Marchisio (2018).

6. References

Alexeenko A.A., Ganguly A., Nail S.L., Computational analysis of fluid dynamics in pharmaceutical freeze-drying, J. Pharm. Sci. 98(9) (2009), 3483–3494. [DOI: 10.1002/jps.21862]

Babac G., Reese J.M., Molecular dynamics simulation of classical thermosize effects, Nanoscale Microscale Therm. Eng. 18(1) (2014), 39-53. [10.1080/15567265.2013.836692]

Barresi A., Overcoming common scale-up issues, Pharm. Technol. Eur. 23(7) (2011), 4-8. [available at http:\\www.pharmtech.com\barresi]

Barresi A.A., Marchisio D.L., Computational Fluid Dynamics data for improving freeze-dryers design, Data Brief (2018), submitted.

Barresi A.A., Pisano R., Freeze drying: Scale-up considerations, in: J. Swarbrick (Ed.), *Encyclopedia of Pharmaceutical Science and Technology*, 4th ed., CRC Press (Taylor and Francis Group), New York, 2013, pp. 1738-1752. [DOI 10.1081/E-EPT4-120050279]

Barresi A.A., Pisano R., Rasetto V., Fissore D., Marchisio D.L., Galan M., Model-based monitoring and controlling of industrial freeze-drying processes, in: B. N. Thorat, (Ed.), *Drying 2008 - Proceedings of the 16th International Drying Symposium (IDS2008)*, Hyderabad, India, 9-12 November 2008a, Vol. B, pp. 746-754.

Barresi A.A., Rasetto V., Marchisio D.L., Fissore D., Pisano R., 2008b, Understanding, monitoring and control the freeze drying process by means of model based tools and Computational Fluid Dynamics, presented at *ISPE Barcelona Conference on Applying a Science and Risk-based Approach*, Barcelona, Spain, 1-4 December 2008.

Barresi A.A., Velardi S.A., Pisano R., Rasetto V., Vallan A., Galan M., In-line control of the lyophilization process. A gentle PAT approach using software sensors, Int. J. Refrigeration 32 **(**2009), 1003-1014. [DOI: 10.1016/j.ijrefrig.2008.10.012]

Barresi A.A., Pisano R., Rasetto V., Fissore D., Marchisio D.L., Model-based monitoring and control of industrial freeze-drying processes: Effect of batch nonuniformity. Drying Technol. 28(5) (2010a), 577-590. [DOI: 10.1080/07373931003787934]

Barresi A.A., Fissore D., Marchisio D.L., Process Analytical Technology in industrial freeze-drying, in: L. Rey and J. C. May (Eds.), *Freeze-Drying/Lyophilization of Pharmaceuticals and Biological Products*, 3rd rev. Edition, Informa Healthcare, New York, 2010b, Chap. 20, pp. 463-496.

Barresi A.A., Pisano R., Fissore D., Advanced control in freeze-drying, in: A. Martynenko, A. Bück, (Eds.), *Intelligent Control in Drying*, CRC Press LLC, 2018, in press.

Batchelor G.K., *An Introduction to Fluid Dynamics*, Cambridge University Press, Cambridge, U.K., 1965.

Bird G.A., *Molecular Gas Dynamics and the Direct Simulation of Gas Flows*, Oxford University Press, Oxford, U.K., 1994.

Bosca S., Fissore D., Demichela M., Risk-based design of a freeze-drying cycle for pharmaceuticals, Ind. Eng. Chem. Res. 54(51) (2015), 12928-12936. [DOI: 10.1021/acs.iecr.5b03719]

Bosca S., Fissore D., Demichela M., Reliability assessment in a freeze-drying process, Ind. Eng. Chem. Res. 56(23) (2017), 6685−6694. [DOI:10.1021/acs.iecr.7b00378]

Docherty S.Y., Borg M.K., Lockerby D.A., Reese J.M., Multiscale simulation of heat transfer in a rarefied gas, Int. J. Heat Fluid Flow 50 (2014), 114-125. [10.1016/j.ijheatfluidflow.2014.06.003]

Elia A.M., Barresi A.A., Intensification of transfer fluxes and control of product properties in freeze-drying, Chem. Eng. Process. 37(5) (1998), 347-358. [DOI: 10.1016/S0255-2701(98)00049-X]

Fissore D., Barresi A.A., In-line product quality control of pharmaceuticals in freeze-drying processes, in: E. Tsotsas, A.S. Mujumdar (Eds.), *Modern Drying Technology Vol. 3: Product Quality and Formulation*, Wiley-VCH Verlag GmbH & Co. KGaA, Weinhein, Germany, 2011a, Chap. 4, pp. 91-154. [ISBN 978-3527-31558-1].

Fissore D., Barresi A.A., Scale-up and process transfer of freeze-drying recipes, Drying Technol. 29(14) (2011b), 1673-1684). [DOI: 10.1080/07373937.2011.597059]

Fissore D., Pisano R., Velardi S.A., Barresi A.A., Galan M., PAT Tools for the optimization of the freeze-drying process, Pharm. Eng. 29(5) (2009), 58-70.

Fissore D., Pisano R., Barresi A.A., On the methods based on the Pressure Rise Test for monitoring a freeze-drying process, Drying Technol. 29(1) (2011), 73-90. [DOI: 10.1080/07373937.2010.482715]

Fissore D., Pisano R., Barresi A.A., A model-based framework for the analysis of failure consequences in a freeze-drying process, Ind. Eng. Chem. Res. 51(38) (2012a), 12386-12397. [DOI: ie-2012-00505n]

Fissore D., Pisano R., Barresi A.A., A model based framework to optimize pharmaceuticals freeze-drying, *Drying Technol.* 30 (2012b), 946-958. [DOI: 10.1080/07373937.2012.662711]

Fissore D., Pisano R., Barresi A.A., Using mathematical modeling and prior knowledge for QbD in freeze-drying processes, in: F. Jameel, S. Hershenson, M. A. Khan, S. Martin-Moe (Eds), *Quality by Design for Biopharmaceutical Drug Product Development*, *AAPS Advances in the Pharmaceuticals Sciences Series 18*, Springer Science+Business Media, New York, 2015, Chap. 23, pp. 565-593. [DOI: 10.1007/978-1-4939-2316-8_23]

Fissore D., R. Pisano, Barresi A.A., Process Analytical Technology for monitoring pharmaceuticals freeze-drying: A comprehensive review. Drying Technol. (2018), in press. [DOI: 10.1080/07373937.2018.1440590]

Ganguly A., Alexeenko A.A., Modeling and measurements of water–vapor flow and icing at low pressures with application to pharmaceutical freeze-drying, Int. J. Heat Mass Transfer 55 (2012) 5503–5513. [DOI: 10.1016/j.ijheatmasstransfer.2012.05.021]

Ganguly A., Rhoden A., Mass spectrometry in freeze drying, over 25 years since the first installation: How far have we come?, presented at *ISL-FD 8th International Conference*, La Habana, Cuba, 24-28 April 2017.

Ganguly A., Venkattraman A., Alexeenko A.A., Simulations of vapor/ice dynamics in a freeze-dryer condenser, presented at *27th Int. Symp. on Rarefied Gas Dynamics*, 2010, in: AIP Conf. Proc. 1333 (2011), pp. 254-259. [DOI: 10.1063/1.3562657]

Ganguly A., Nail S.L., Alexeenko A.A., Rarefied gas dynamics aspects of pharmaceutical freeze-drying, Vacuum 86(11) (2012), 1739–1747. [10.1016/j.vacuum.2012.03.025]

Ganguly A., Alexeenko A.A., Schultz S.G., Kim S.G., Freeze-drying simulation framework coupling product attributes and equipment capability: Toward accelerating process by equipment modifications, Europ. J. Pharm. Biopharm. 85(2) (2013), 223-235. [DOI:10.1016/j.ejpb.2013.05.013]

Ganguly A., Varma N., Sane P., Bogner R., Pikal M., Alexeenko A. Spatial variation of pressure in lyophilization product chamber part 1: Computational modeling, AAPS PharmSciTech 18(3) (2017), 577–585. [DOI: 10.1208/s12249-016-0513-3]

Genin N., Rene F., Corrieu G., A method for on-line determination of residual water content and sublimation end-point during freeze-drying, Chem. Eng. Proc. 35(4) (1996), 255-263. [10.1016/0255-2701(95)04131-1]

Grad H., On the kinetic theory of rarefied gases, Comm. Pure Applied Math. 2(4) (1949), 331-407. [DOI: 10.1002/cpa.3160020403]

Hill J.E., Sunderland J.E., Sublimation-dehydration in the continuum, transition and free-molecule flow regimes, Int. J. Heat Mass Transfer 14(4) (1971), 625-638. [DOI: 10.1016/0017-9310(71)90011-1]

Icardi M., Asinari P., Marchisio D.L., Izquierdo S., Fox R.O., Quadrature-based moment closures for non-equilibrium flows: Hard-sphere collisions and approach to equilibrium, J. Comp. Phys. 231(21) (2012) 7431-7449. [DOI: 10.1016/j.jcp.2012.07.012]

Jennings T.A., Transferring the lyophilization process from one freeze-dryer to another, Am. Pharm. Rev. 5 (2002), 34-42.

Knudsen M., Die Gesetze der Molekularströmung und der inneren Reibungsströmung der Gase durch Röhren, Annal. Physik 333 (1909), 75–130.

Kumagai H, Nakamura K., Yano T., Rate analysis of freeze drying of a model system by a Uniformly Retreating Ice Front model, Agric. Biol. Chem. 55(3) (1991), 731-736. [DOI: 10.1080/00021369.1991.10870659]

Marchisio D.L., Fox R.O., *Computational Models for Polydisperse Particulate and Multiphase Systems*, Cambridge University Press, Cambridge, U.K., 2013.

Marchisio D.L., Galan M., Barresi A.A., Use of Computational Fluid Dynamics for improving freeze-dryers design and understanding. Part 2: Condenser duct and valve modelling, Europ. J. Pharm. Biopharm., this issue.

Maxwell J.C., On stresses in rarified gases arising from inequalities of temperature. Phil. Trans. Royal Soc. London 170 (1879), 231–256.

Mayeresse Y., Veillon R., Sibille P.H., Nomine C., Freeze-drying process monitoring using a cold plasma ionization device, PDA J. Pharm. Sci. Technol. 61(3) (2007), 160-174.

Mellor J.D., *Fundamentals of Freeze-Drying*, Part 2: Cyclic-Pressure Operation, Academic Press, London, 1978.

Milton N., Pikal M.J., Roy M.L., Nail S.L., Evaluation of manometric temperature measurement as a method of monitoring product temperature during lyophilization. PDA J. Pharm. Sci. Technol. 51(1) (1997), 17-24.

Nail S.L., Searles J.A., Elements of quality by design in development and scale-up of freeze-dried parenterals, Biopharm. Int. 21 (2008), 44–52.

Nurlybaev N.A., Discrete velocity method in the theory of kinetic equations, Transport Theory Stat. Phys., 22(1) (1993), 109-119. [DOI: 10.1080/00411459308203533]

Oetjen G.W., *Freeze-Drying*, Wiley-VHC, Weinheim, Germany, 1999.

Patel S.M., Chaudhuri S., Pikal M.J., Choked flow and importance of Mach I in freeze-drying process design. Chem. Eng. Sci. 65(21) (2010), 5716–5727. [10.1016/j.ces.2010.07.024]

Petitti M., Barresi A.A., Marchisio D.L., CFD modelling of condensers for freeze-drying processes. Sādhanā (Bangalore) – Acad. Proc. Eng. Sci. 38(6) (2013), 1219–1239. [DOI:10.1007/s12046-013-0155-z]

Pisano R., Rasetto V., Petitti M., Barresi A.A., Vallan A., Modelling and experimental investigation of radiation effects in a freeze-drying process, in F. Scura, M. Liberti, G. Barbieri, E. Drioli (Eds), *Abstracts of the 5th Chemical Engineering Conference for Collaborative Research in Eastern Mediterranean Countries EMCC5*, Cetraro (CS), Italy, 24-29 May 2008, pp. 394-398.

Pisano R., Fissore D., Barresi A.A., Heat transfer in freeze-drying apparatus, in M.A. dos Santos Bernardes *(Ed), Developments in Heat Transfer*, InTech, Rijeka, Croatia, 2011a, Chap. 6, pp. 91-114. [ISBN 978-953-307-569-3] Open access book, available at http://www.intechopen.com/books/show/title/developments-in-heat-transfer.

Pisano R., Fissore D., Barresi A.A., Innovation in monitoring food freeze-drying, Drying Technol. 29(16), (2011b), 1920–1931. [DOI: 10.1080/07373937.2011.596299]

Pisano R., Fissore D., Barresi A.A., In-line and off-line optimization of freeze-drying cycles for pharmaceutical products, *Drying Technol*. 31(8) (2013), 905-919. [DOI: 10.1080/07373937.2012.718307]

Pisano R., Ferri G., Fissore D., Barresi A.A., Freeze-drying monitoring via Pressure Rise Test: the role of pressure sensor dynamics, in *Proc. IEEE International Instrumentation and Measurements Technology Conference "I2MTC 2017"*, Torino, Italy, 22-25 May 2017, pp. 1282-1287 (article nr 17039663). [DOI: 10.1109/I2MTC.2017.7969892]

Rasetto V., Use of mathematical models in the freeze-drying field: process understanding and optimal equipment design, PhD Diss, Politecnico di Torino, Italy, 2009.

Rasetto V., Marchisio D.L., Fissore D., Barresi A.A., Model-based monitoring of a non-uniform batch in a freeze-drying process, in: B. Braunschweig & X. Joulia (Eds.), *18th European Symposium on Computer Aided Process Engineering, Computer-Aided Chemical Engineering Series*, Elsevier, Amsterdam, 2008, Vol. 25 (CD Edition), paper FP_00210, 6 pp. [ISBN (CD) 978-0-444-53228-2]

Rasetto V., Marchisio D.L., Barresi A.A., Analysis of the fluid-dynamics of the drying chamber to evaluate the effect of pressure and composition gradients on the sensor response used for monitoring the freeze-drying process, in: *Proceedings of the European Drying Conference AFSIA 2009*, Lyon, France, 14-15 May 2009. *Cahier de l'AFSIA* Nr 23, pp. 98-99.

Rasetto V., Marchisio D.L., Fissore D., Barresi A.A., On the use of a dual-scale model to improve understanding of a pharmaceutical freeze-drying process. J. Pharm. Sci. 99(10) (2010), 4337–43550. [DOI: 10.1002/jps.22127]

Sane P., Varma N., Ganguly A., Pikal M., Alexeenko A., Bogner R.H., Spatial variation of pressure in the lyophilization product chamber part 2: Experimental measurements and implications for scale-up and batch uniformity, AAPS PharmSciTech. 18(2) (2017), 369–380. [DOI: 10.1208/s12249-016-0502-6]

Searles J., Observation and implications of sonic water vapour flow during freeze-drying, Am. Pharm. Rev. 7(2) (2004), 58–69.

Sharma C., Malhotra D., Rathore A., Review of computational fluid dynamics applications in biotechnology processes, Biotechnol. Prog. 27(6) (2011), 1497-1510.

Struchtrup H., *Macroscopic Transport Equations for Rarefied Gas Flow: Approximation Methods*, Springer, Berlin, Germany, 2005.

Toei R., Okazaki M., Asaeda M., The stability of plane sublimation and a model of zone sublimation in freeze drying of porous bodies, J. Chem. Eng. Japan 8(4) (1975), 282-288. [DOI: 10.1252/jcej.8.282]

Velardi S.A., Barresi A.A., Development of simplified models for the freeze-drying process and investigation of the optimal operating conditions, Chem. Eng. Res. Des. 86(1) (2008), 9-22. [DOI: 10.1016/j.cherd.2007.10.007]

Velardi S.A., Rasetto V., Barresi A.A., Dynamic Parameters Estimation method: Advanced Manometric Temperature Measurement approach for freeze-drying monitoring of pharmaceuticals solutions, Ind. Eng. Chem. Res. 47(21) (2008), 8445-8457. [DOI:10.1021/ie7017433]

White C., Borg M.K., Scanlon T.J., Longshaw S.M., John B., Emerson D.R., Reese J.M., DsmcFoam+: An OpenFOAM based direct simulation Monte Carlo solver, Comp. Phys. Com. (2017), in press. [DOI: 10.1016/j.cpc.2017.09.03]

Zhang S., Liu J., Distribution of vapor pressure in the vacuum freeze-drying equipment. Math Problems Eng. 2012 (2012), article ID 921254, 10 pp. [DOI: 10.1155/2012/921254].

Appendix.

A. Lumped zero-dimensional model used for the on-the-fly multi-scale approach

The simplified model used in the on-the-fly multi-scale approach is derived from the URIF model (Toei et al., 1975; Kumagai et al., 1991) and is constituted by simple ordinary differential equations. The heat balance equation derived under steady-state (A1) is adopted; equations (A1) and (A3) assume that all the heat, Q, supplied by the heating fluid is used for the sublimation, where the sublimation mass flow can be expressed with Eq. (A2). From Eq. (A4), obtained substituting into Equation (A1), the product temperature at the bottom can be obtained if the global heat transfer coefficient K_v and mass transfer coefficient R_p are known.

$$\frac{dQ}{dt} = A_{vial} K_v \left(T_{shelf} - T_B \right) = \dot{m}_{sub} \Delta H_{sub} \tag{A1}$$

$$\dot{m}_{sub} = \frac{1}{R_p} A_p \left(p_i - P_c \right) \tag{A2}$$

$$\frac{dQ}{dt} = \frac{1}{R_p} A_p \left(p_i - P_c \right) \Delta H_{sub} \tag{A3}$$

$$\frac{1}{R_p} A_p \left(p_i - P_c \right) \Delta H_{sub} = A_{vial} K_v \left(T_{shelf} - T_B \right) \tag{A4}$$

p_i, the vapour pressure at the sublimation interface at the temperature T_i, is expressed by the equilibrium law (A5). Substituting equation (A5) in equation (A4), equation (A6) is obtained,

$$p_i = \exp\left(\frac{6140.4}{T_i} + 28.916 \right) \tag{A5}$$

$$\exp\left(\frac{6140.4}{T_i} + 28.916 \right) - \frac{A_{vial}}{A_p} \frac{R_p K_v}{2687.4 \cdot 10^3} \left(T_{shelf} - T_B \right) + P_c \tag{A6}$$

$$T_B = T_i + \Delta T \tag{A7}$$

where P_c is the pressure in chamber and is directly computed by the CFD simulation, while T_B is the bottom temperature of the product and can be estimated by equation (A7); A_{vial} and A_p are the vial bottom and product section.

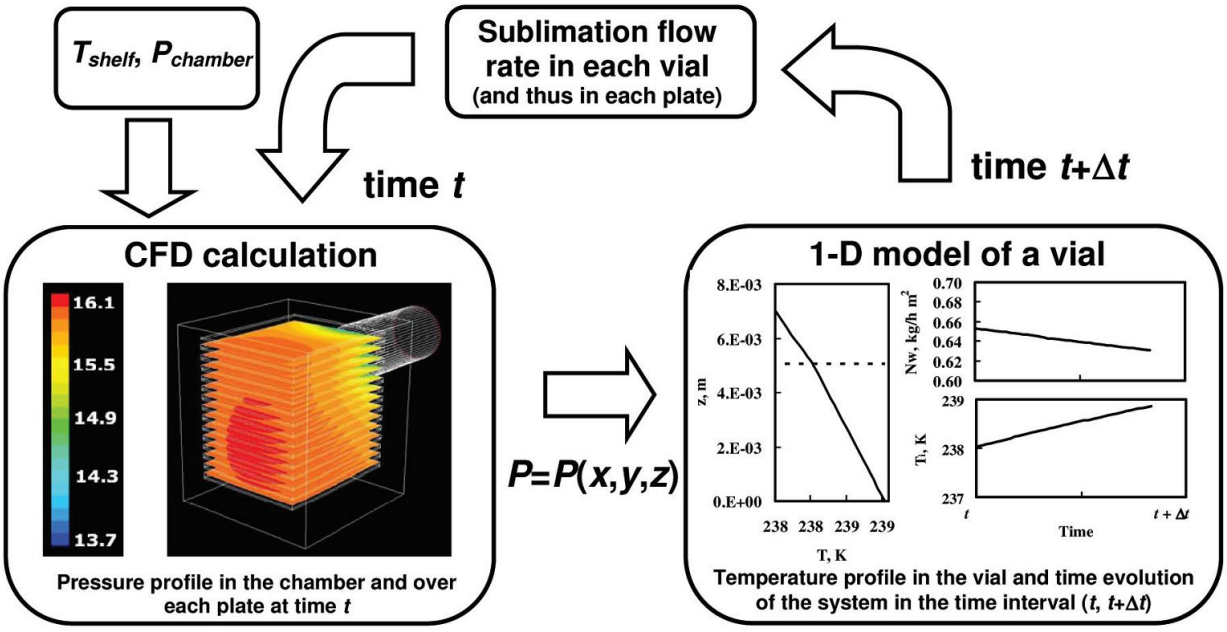

Figure 1. Scheme of the multi-scale off-line approach (FIMM). In the left inset the 3D contour plot of the pressure (in Pa) over the shelves of the industrial apparatus (L1; the data shown refer to 1 kg h^{-1} m^{-2} sublimation rate for an outlet pressure of 10 Pa). In the right inset an example of the evolution of the position of the interface (z), of the vial sublimation flux and of the product temperature at the ice-dried layer interface (T_i).

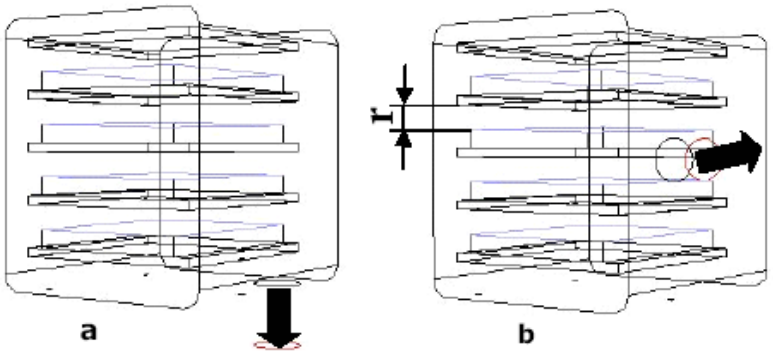
r
a
b

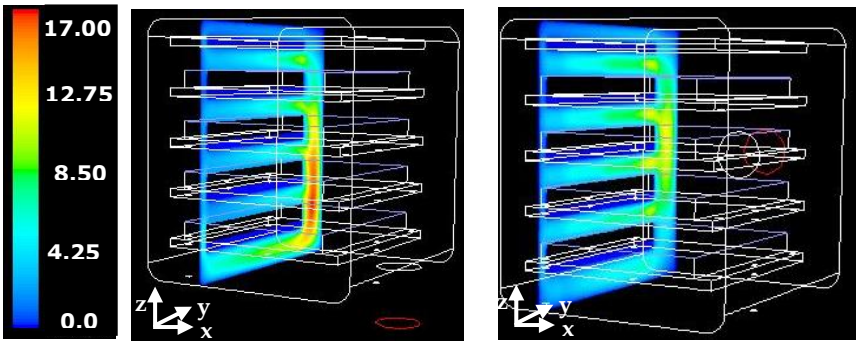
17.00
12.75
8.50
4.25
0.0
z
y
x
z
y
x

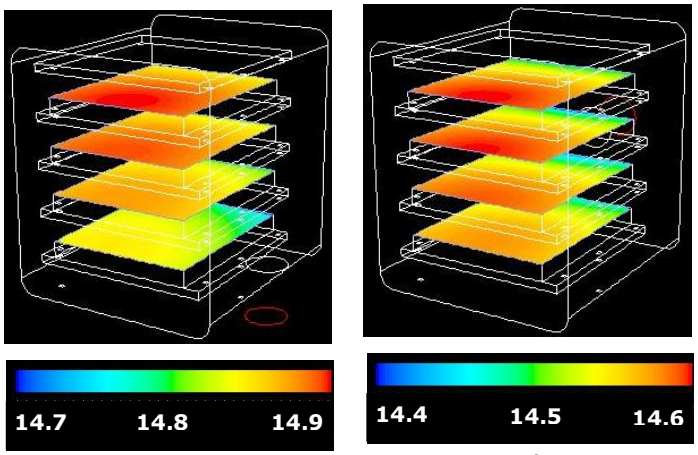
14.7
14.8
14.9
14.4
14.5
14.6

***r*= 57 mm**

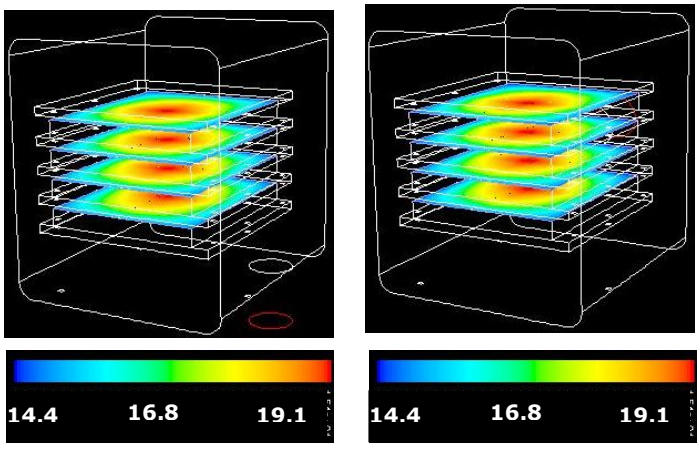
14.4
16.8
19.1
14.4
16.8
19.1

***r*= 7 mm**

Figure 2. Upper graphs: 3D representation of the small freeze-dryer chamber with the duct in different positions: bottom (a), and in the centre of the rear wall (b). The slab that represents the volume occupied by trays or vials is shown, and the size of the free clearance *r*, is evidenced. Velocity magnitude (m/s) plotted on *y*-*z* plane (middle graphs) for the S1 case (r = 57 mm) for the two configurations.
On the two bottom rows, the contour plots of the absolute pressure (in Pa) over the vapour sources for two shelf clearances are shown (cases S1, and S3). A mass flow rate equal to $4.5 \cdot 10^{-5}$ kg s^{-1}, and outlet pressure 10 Pa, corresponding to typical values experimentally measured in lab operation has been considered in this case.

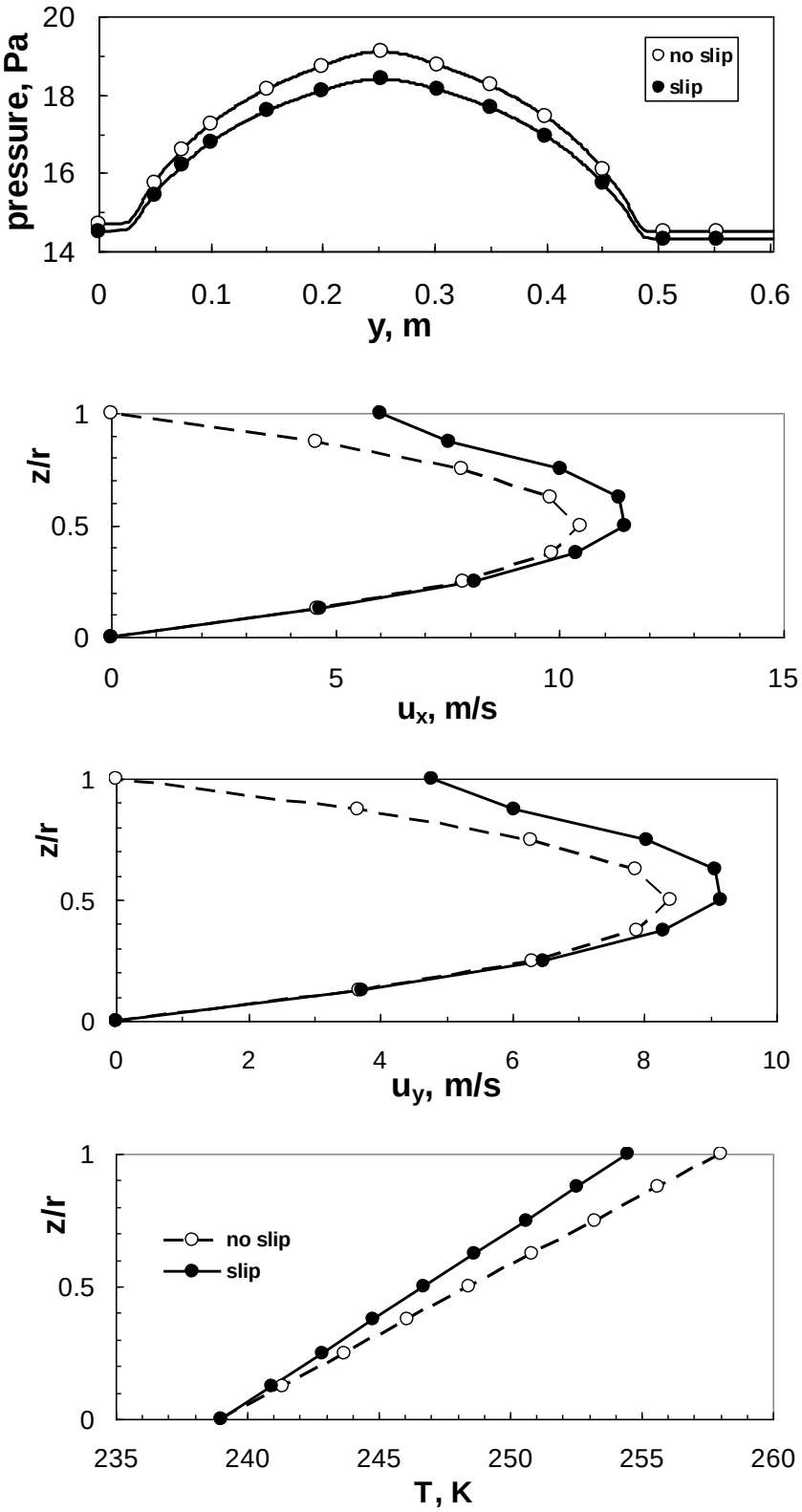

Figure 3. Effect of slip and no-slip boundary conditions. From top to bottom, comparison: of the pressure profiles along the *y* direction, across the whole chamber; of the u_x-velocity component; of the u_y-velocity component; of the temperature. In the clearance of the second shelf (from bottom), along a median line; configuration with rear duct, r = 7 mm.

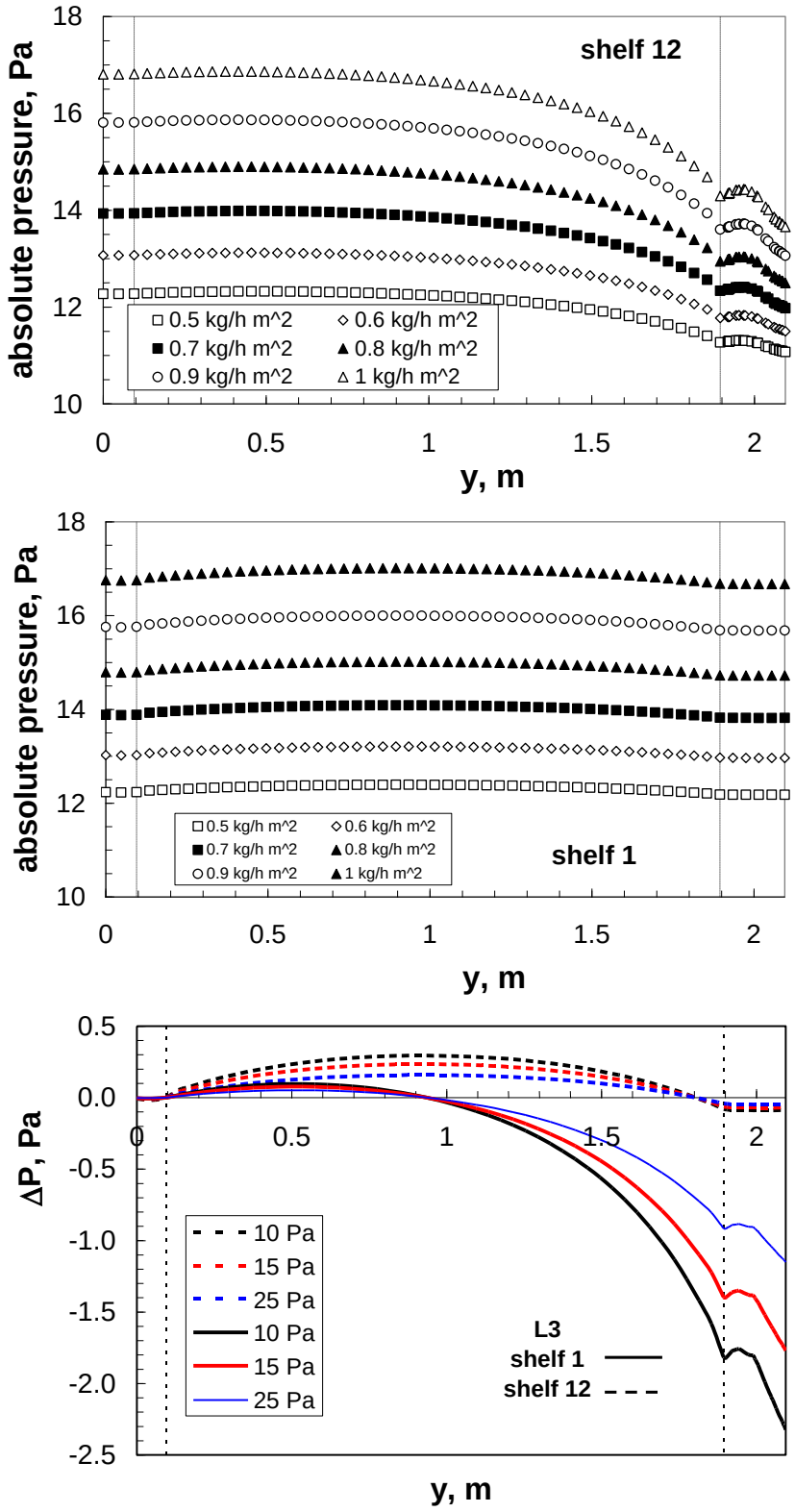

Figure 4. Pressure distribution across the chamber as a function of the sublimation rate for an upper (top graph) and the bottom shelf (middle graph), in the configuration with 15 shelves (L2) (outlet pressure = 10 Pa). The dashed line evidences the limit between the border of the shelf and the lateral clearance zone.
In the bottom graph the dependence on total pressure (fixed at the outlet) is shown, for two different shelves: shelf 1 (dashed lines); shelf 12 (continuous line). L3 configuration, with 16 active shelves, sublimation rate = 0.7 kg h^{-1} m^{-2}.

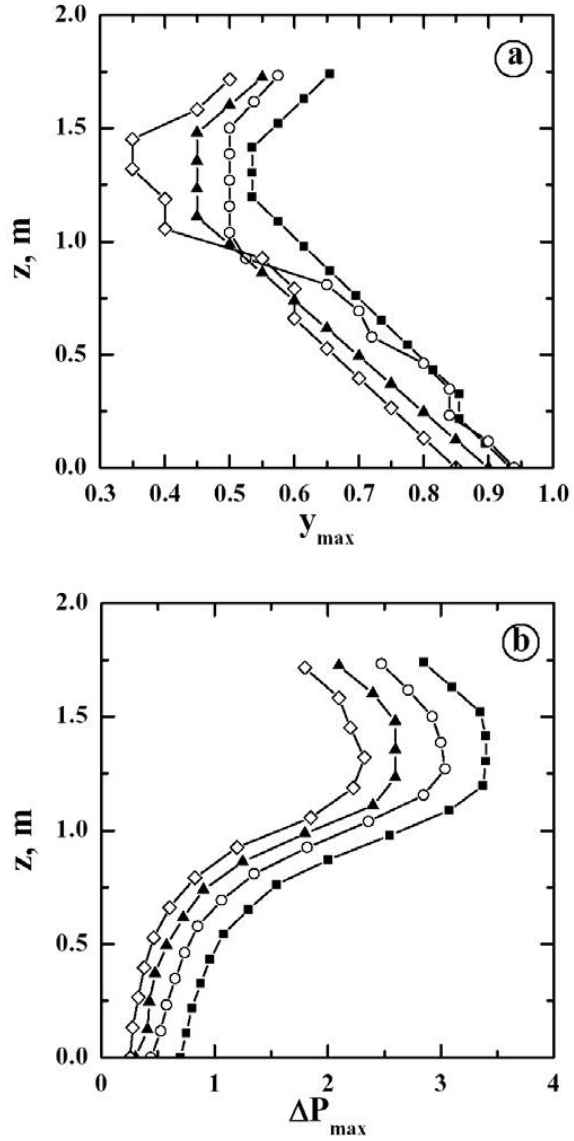

Figure 5. Variation in the location of the maximum of the pressure value along the shelf in the *y* direction, y_{max} (a), and maximum pressure variation ΔP_{max} (b), as a function of the *z*-coordinate for the four configurations of the large scale freeze-dryer, with 1 kg $h^{-1}m^{-2}$ sublimation flux: ◇, L1; ▲, L2; ○, L3; ■, L4.

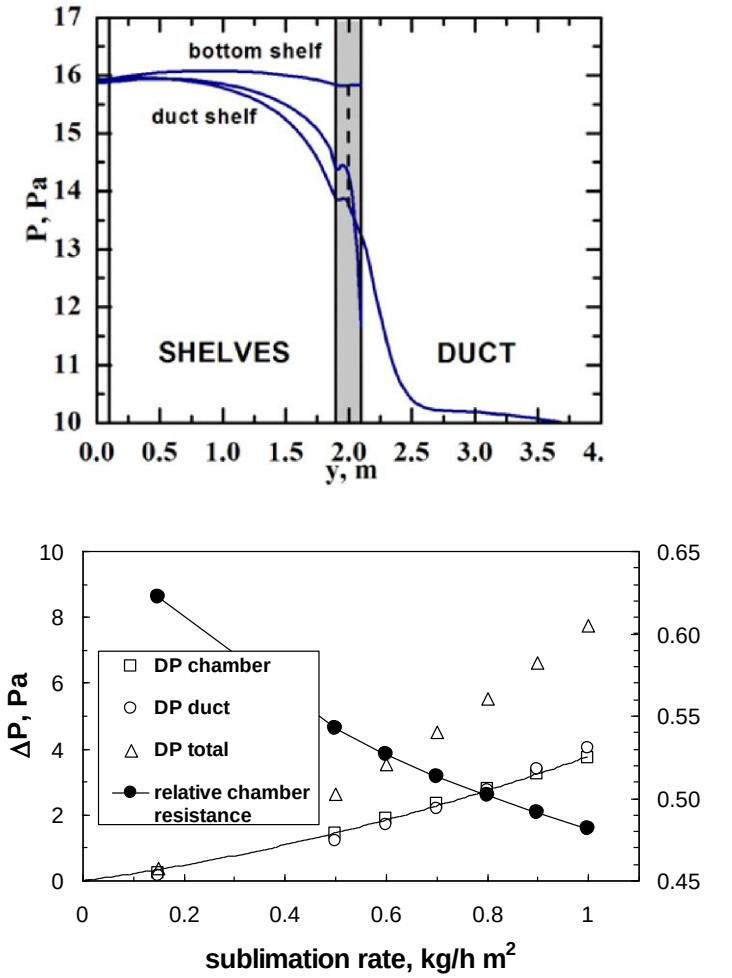

Figure 6. Upper graph: pressure gradients in the drying chamber and in the duct for three shelves (the shelf at the bottom of the chamber, close to the duct and at the top of the chamber); the grey zone corresponds to the clearance between wall and shelves. L1 configuration, J_w = 1 kg h^{-1} m^{-2}. Lower graph: contribution to total pressure drop of shelves, chamber, duct inlet for fifferent sublimation rates; L3 configration.

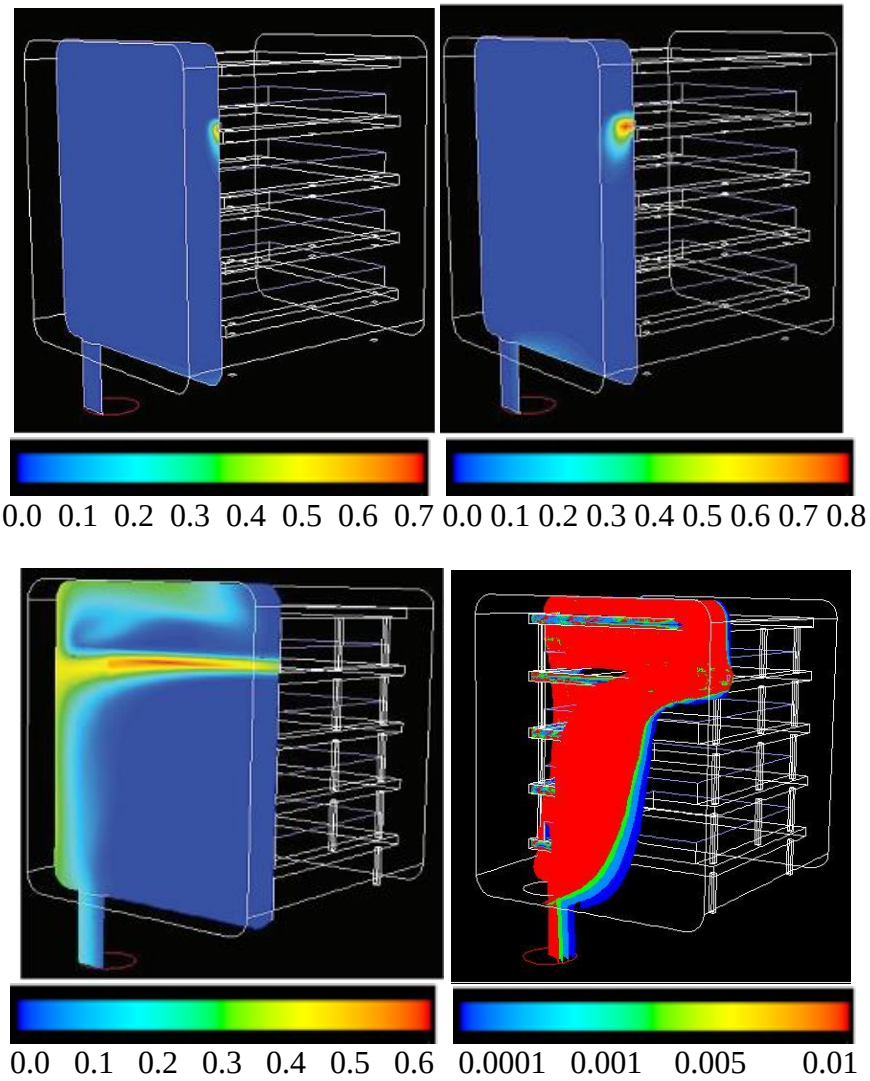

Figure 7. Inert gas mass fraction distribution in the small scale drying chamber for different inert gas inlet flow rates: $1.20 \cdot 10^{-7}$ kgs^{-1} (upper left, -); $1.20 \cdot 10^{-6}$ kgs^{-1} (upper right, -); $1.20 \cdot 10^{-5}$ kgs^{-1} (bottom left, -). Red colour corresponds to maximum value for each case, yellow to 75%, green to 50% , light blue to 25% and dark blue to 0, but the scale is different in the various figures. Outlet pressure = 10 Pa; water sublimation rate 1 kg h^{-1} m^{-2}.
In the bottom right image, the zone where the inert gas concentration is higher than the chamber average value is evidenced (total inert gas flow equal to 12% of the water sublimation flow).

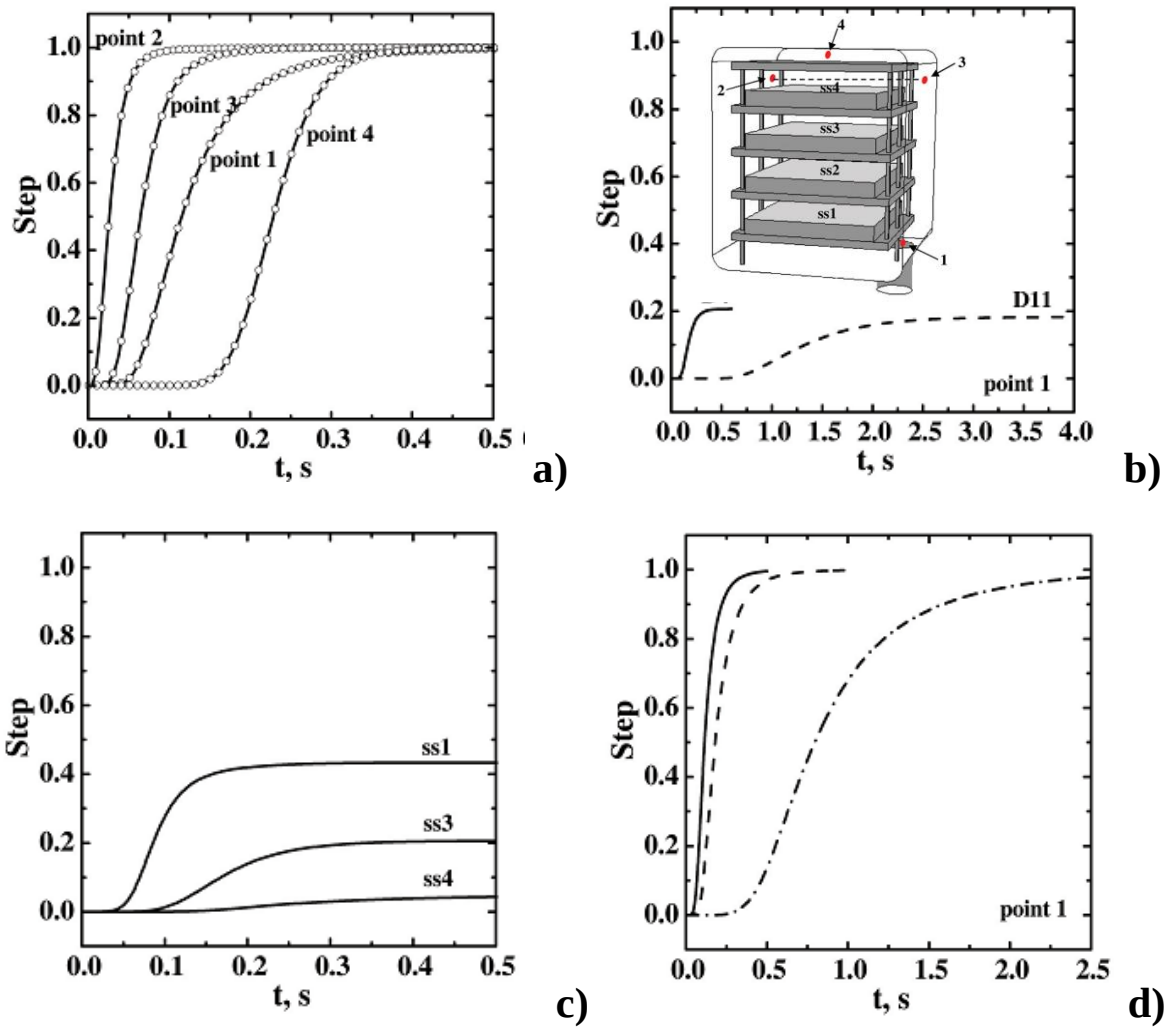

Figure 8. Dynamic response of the small pilot freeze-dryer to disturbances in the sublimation rate of different shelves; the location of the virtual measuring devices is shown in in the inset of graph b).
a) Response in the four detection points; fully loaded system, J_w = 1 kg h^{-1} m^{-2}, with disturbance over all the shelves. Response without species diffusivity (simulation D1, line) and with species diffusivity (D2, symbols) are compared (overlapped curves).
b) Response in the four detection points (but only point 1 is effective); fully loaded system, with disturbance applied only at ss_3. Response at high (J_w = 1 kg h^{-1} m^{-2}, D4, continuous line) and low (J_w = 0.1 kg h^{-1} m^{-2}, D11, dashed line) sublimation rate are compared.
c) Response in detection point 1; fully loaded system, J_w = 1 kg h^{-1} m^{-2}, with disturbance applied only to one of the shelves: ss_1 (D3), ss_3 (D4), ss_4 (D6).
d) Response in detection point 1; fully loaded system, with disturbance over all the shelves. Different sublimation rates are compared: ––, J_w = 1 kg h^{-1} m^{-2} (D1); - - -, J_w = 0.5 kg h^{-1} m^{-2}, (D8); –·–, J_w = 0.1 kg h^{-1} m^{-2}, (D9).

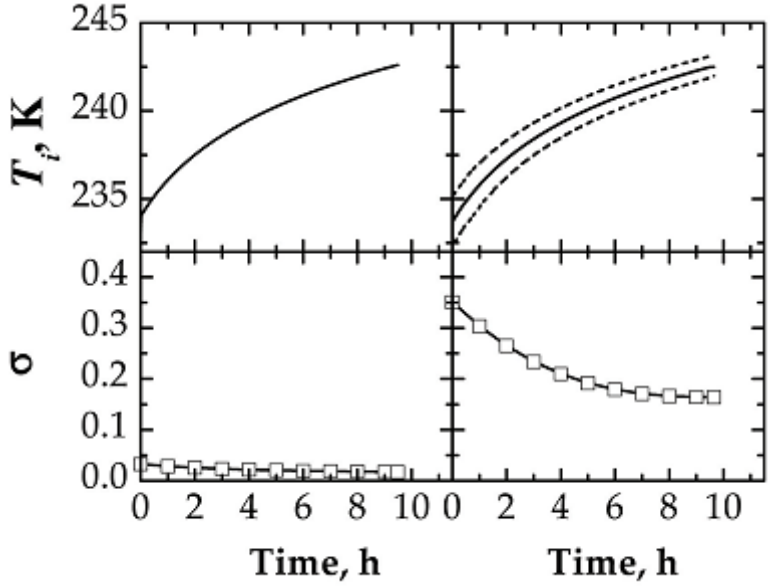

Figure 9. Time evolution of the mean value of interface temperature, T_i (upper graphs, solid line) and of the standard deviation, σ (lower graphs) for the vials on the 1st (left side) and on the 12th (right side) shelf (configuration L3). Dashed lines identify the upper and lower bound of the interface temperatures in the vials. Solution of bovine serum albumin; frozen product thickness = 7.2 mm, shelf temperature = 258 K, reference chamber pressure =10 Pa.

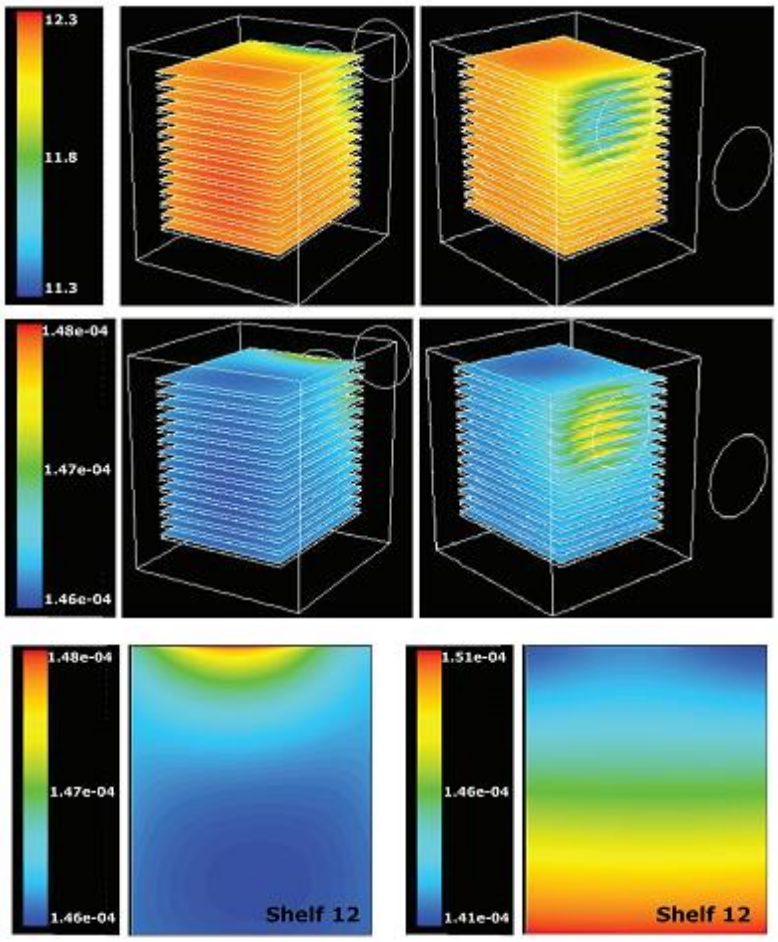

Figure 10. Contour plots of absolute pressure (Pa, top graphs) and mass sublimation flux (kg s^{-1} m^{-2}, middle graphs) for the configuration L1, with constant shelf temperature (258 K); front and back side views are shown. In the bottom graphs the detail of the mass sublimation flux over the 12^{th} shelf is shown for the configuration L1 with (left) constant heating fluid temperature and (right) a 2°C linear variation of the heating fluid temperature.